COMPUTATIONAL METHOD TO ANALYZE NOVEL INDUSTRIAL-TYPE COMPACT HEAT EXCHANGERS FIN DESIGNS

by

OLUWATOSIN SAMUEL AWORANTI

A Dissertation Submitted in

Partial Fulfilment of the

Requirements for the Degree of

DOCTOR OF PHILOSOPHY

in Engineering

at

The **University of Wisconsin-Milwaukee**

May 2022

ABSTRACT

COMPUTATIONAL METHOD TO ANALYZE NOVEL INDUSTRIAL-TYPE COMPACT HEAT EXCHANGERS FIN DESIGNS

by

Oluwatosin Samuel Aworanti

The University of Wisconsin-Milwaukee, 2022
Under the Co-Supervision of Professor Kevin Renken and Professor John Reisel

In this study, the computational fluid dynamics (CFD) method of numerical simulations has been applied to determine the heat load and pressure drop characteristics of computational method to analyze novel industrial-type compact heat exchangers fin designs. Two CFD software programs, Ansys Fluent and STAR-CCM+, were tested with air laminar flow. The research work demonstrated that Ansys Fluent is the more sensitive CFD software to laminar flow out of the two. Seven fin designs were tested to evaluate their performance in compact heat exchangers.

The friction factor, *f*, and the Chilton Colburn factor, *j*, were used as the primary measures of performance. It was found that designs with the lower levels of velocity streamline disturbance, give lower friction factor while the highest Chilton Colburn factors, j, are produced by particular interactions between the fluid flow and the fin. As expected, for all the designs, the friction factor *f* decreases with an increase in Reynolds number while the plot of Chilton Colburn factor *j* increases by either no amount or a small amount with an increase in Reynolds number. It is was also found that a finer mesh size plays an important role the analysis of the thermophysical characteristics of the fin design. Finer mesh size result in more accuracy in the prediction of heat load and pressure drop results.

DEDICATIONS

First, I dedicate this work to God almighty for the grace to go through this program successfully. A big thank you to my advisors, Dr. Kevin Renken and Dr. John Reisel, for the opportunity to grow in research and writing under your supervisions. They have pushed me towards full potential and I appreciate it.

Temi, my love and life, you have supported me every step of the way. Countless late nights of studying, skipped vacations, stress, tears, and more; you have stood by me through the sacrifices and grounded me through it all. I would not be where I am today without your encouragement and support. You have helped me to become a man worthy of your love in personal growth, in character, and ethic.

A thank you to the countless other professors, my committee members, who encouraged the best in not just me, but all students by being true teachers. To my peers, classmates, and my undergraduate team, no person or student can function alone. It is the individual who puts the work in, but it is those around them that help keep the pace.

Finally, to my parents, though you're not here to see it, I admit that I couldn't avoid following in your footsteps. Everything I am today stems from what am being taught in terms of work ethic and of character. I will continue forward, doing my best, knowing that you all, are proud of me.

TABLE OF CONTENTS

LIST OF FIGURES

LIST OF TABLES

LIST OF SYMBOLS

Symbols	Description	Units
a	amplitude	m
A_S	surface area	m^2
A_c	cross-section area	m^2
C_p	specific heat capacity	$\frac{J}{kg \cdot K}$
D	diameter	m
D_h	hydraulic diameter	m
f	Fanning friction factor	
j	Chilton-Colburn factor	
h	convection heat transfer coefficient	$\frac{W}{m \cdot ℃}$
H	fin height	m
L	fin length	m
L	length of test piece	m
$\dot{m}$	mass flow rate	$\frac{kg}{s}$
t	fin thickness	m
$\overrightarrow{u}$	velocity field	
ν	kinematic viscosity	$\frac{m^2}{s}$

μ	dynamic viscosity	$\frac{kg}{m \cdot s}$
ρ	density	$\frac{kg}{m^3}$
k	thermal conductivity	$\frac{W}{m \cdot K}$
λ	wavelength	m
n	fin frequency	$\frac{1}{m}$
τ	shear stress	Pa
v	inlet velocity	$\frac{m}{s}$
V_{avg}	average velocity	$\frac{m}{s}$
ε	effectiveness	
W	fin external width	m
B1	hole spacing	m
Δp	pressure drop	Pa
T_w	wall temperature	K
T_∞	fluid temperature	K
∇	Hamiltonian operator	

Subscripts

w	wall
∞	fluid
I	imaginary face/edge/cell

Abbreviations

Al	aluminum	
BAHX	brazed Aluminium Heat Exchanger	
CAD	computer aided design	
CFD	computational fluid dynamics	
DAQ	data acquisition software	
FMG	full multigrid	
FPI	frequency per inch	
MINLP	mixed-integer nonlinear programming	
MS	mesh size	m
NL	notch length	m
NTU	number of transfer units	
O	offset	

PFHE	plate fin heat exchanger
Pr	Prandtl number
R	rectangular
Re	Reynolds number
S	single
Si	silicon
St	Stanton number

CHAPTER ONE

1.0 INTRODUCTION

A heat exchanger is a device that transfers thermal energy between two or more fluids, one comparatively hot and the other comparatively cold which are typically classified according to flow arrangement (Raju, 2011). In the heat exchanger, there are usually no external heat and work interactions (Shah R. K., 2007). The most common classes are the parallel flow, counterflow and cross flow (finned with both fluids unmixed or unfinned with one fluid mixed and the other unmixed). In the parallel-flow arrangement, the hot and cold fluids enter at the same end, flow in the same direction, and leave at the same end, while in the counterflow arrangement, the fluids enter at opposite ends, flow in opposite directions, and leave at opposite ends (Bergman, 2017). In many heat exchangers, the fluids are separated by a heat transfer surface and ideally do not mix or leak. According to Shah (2007), sensible heat exchangers are heat exchanger with no phase change in any of its fluids.

1.1 INTRODUCTION TO COMPACT HEAT EXCHANGERS

The design optimization of compact heat exchangers fin designs leads to an improvement in the efficiency and performance of these integrated energy systems. Compact heat exchangers are known for a high heat output at a comparatively small input of both uniform and non-uniform work with temperature differences.

The closer the contact between the two fluids, the more compact the heat exchanger. Szücs (1962) also simplified the heat transfer process into three steps:

1. the thermal energy from the inside of the warmer fluids flows into the solid retaining wall;

2. the thermal energy then passes by conductance through the wall that separates the two fluids; and
3. the thermal energy from the wall-side boundary of the colder fluid, reaches the inside of the colder stream.

The performance of heat exchangers is largely affected by fin geometries. Common types of geometries are plain, wavy, serrated/offset trip, louvered and perforated fin structure as shown in Figure 1.1. Compact heat exchangers have dense arrays of finned tubes or plates. These are typically used when at least one of the fluids is a gas; gases lead to a small convection heat transfer coefficient and need a very large heat transfer area per volume to achieve a very adequate heat transfer.

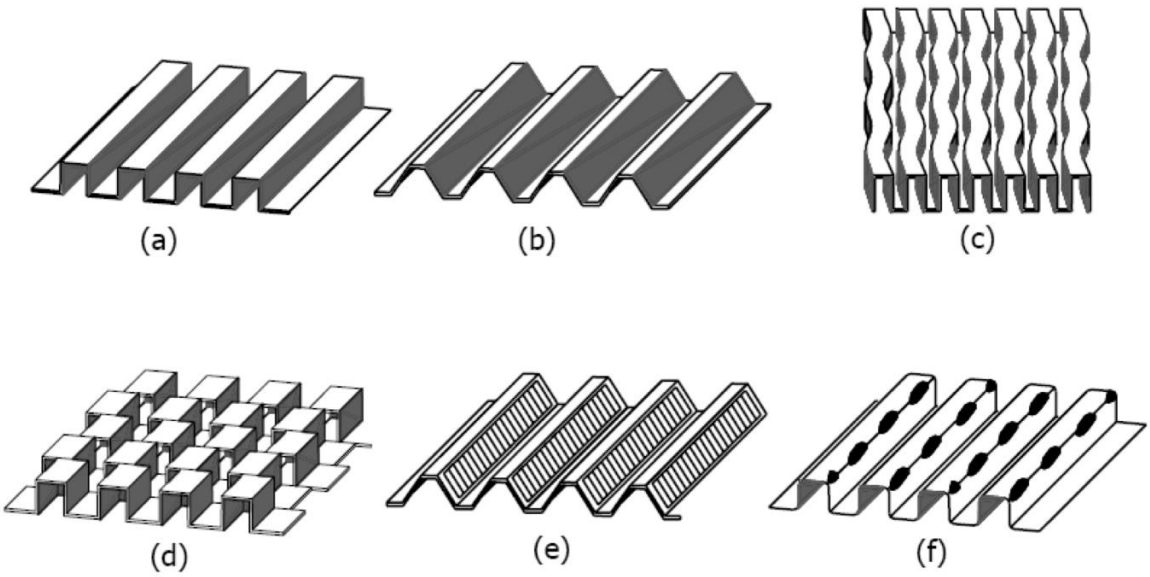

Figure 1.1: Types of fin surfaces: (a) plain rectangular, (b) plain trapezoidal, (c) wavy, (d) serrated or offset strip, (e) louvered, (f) perforated.

The calls for energy conservation at industrial plants have led to the continuous analysis of heat flow systems, leading to the replacement of existing heat exchangers to newly-developed ones or in the installation of heat recovery exchangers. Alternatively, the feasibility of using organic fluid Rankine cycles has been tested at steel plants to tap energy of exhaust gases (Shah R. K., 2007).

Plate fin heat exchangers (PFHE) were first conceived in 1923 for the food industry. Compared to shell-and -tube heat exchangers of the same capacity, PFHEs are believed to weigh about 75 percent less (Lee H. , 2010). They are typically built of thin metal plates, which are either smooth or have some form of corrugation. Generally, these heat exchangers can accommodate high fluid pressures (over 3MPa) and can operate at a range of temperatures from cryogenic up to ultrahot. As shown in Figure 1.2, the basic elements of plate fin heat exchangers is displayed.

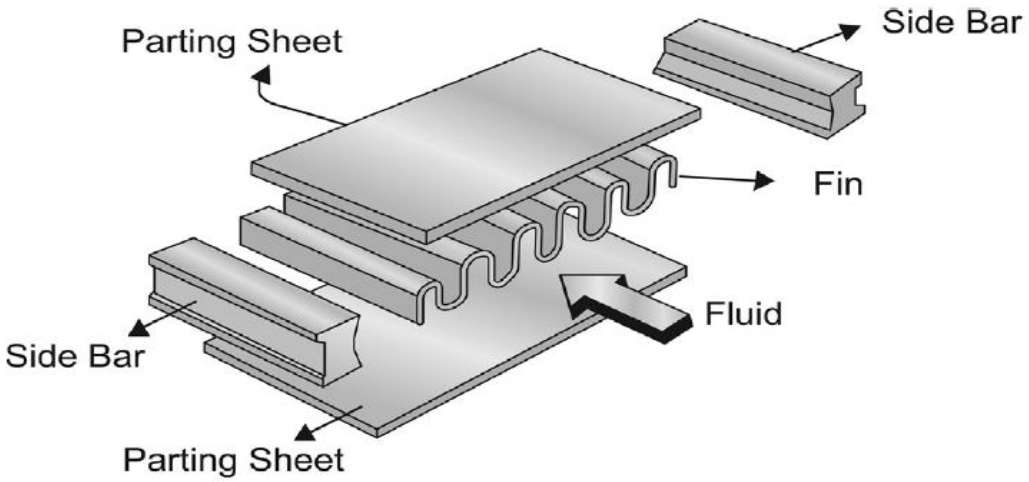

Figure 1.2: Basic elements of plate-fin heat exchanger (Guo, 2014).

Due to their high efficiency and compact structures, plate-fin heat exchangers (PFHEs) are used in process industries, power engineering, aerospace applications, electronics, automobiles, cryogenics and air-conditioning systems. PFHEs reduce energy consumption and material costs

(Huizhu, 2018). The either corrugated or embossed plates are packed to form channel passages for flow (Raju, 2011). There are two types of plate-fin heat exchangers. One is the plate-and-frame or gasketed plate heat exchanger and the other is a welded or brazed plate heat exchanger. The gasketed plate heat exchanger is designated to accommodate a mounted mechanical cleaning device. Hence, this type of exchanger is appropriate for situations requiring frequent cleaning, such as in food processing. One of the problems with the gasketed plate heat exchangers is the presence of gaskets, which limits operating temperatures and pressures.

In recent years, it has become increasingly apparent that PFHEs are also suitable to the liquid-to-liquid heat transfer processes as well as condensers and evaporators, especially in high power dissipation (Jiawen, 2017; Wei, 2017). Plate-fin heat exchangers have not been widely applied in most process industries is they cannot handle high pressures and temperatures due to material considerations, and that they are normally used for clean and non-corrosive fluids (Taylor, 1990).

Two modes of heat transfer occur in a PFHE: convective heat transfer between the walls (the plates and the fins) and the fluid and conductive heat transfer between the plates through the fins. The overall convective heat-transfer performance of the fins results from the interaction between heat conduction in the section of the fins and heat convection along their surface. Due to this interaction, non-negligible temperature gradients often appear inside the fins that affect the heat transfer.

1.2 TYPES OF FLUID FLOWS

Laminar flows are characterized by smooth streamlines and highly ordered motion which is encountered when highly viscous fluids such as oils flow in small pipes or narrow passages. Turbulent flows exhibit velocity fluctuations and highly disordered motion. Transition flows are conditions where the flow that fluctuates between laminar and turbulent flows.

The transition from laminar to turbulent flow depends on the geometry, surface roughness, flow velocity, surface temperature and the type of fluid. The flow regime depends mainly on the ratio of inertial forces to viscous forces and is characterized by the Reynolds number:

$$Re = \frac{inertia\ forces}{viscous\ forces} = \frac{V_{avg}\,D}{\nu} = \frac{\rho V_{avg} D}{\mu} \qquad (1.1)$$

where, V_{avg} = average velocity

D = diameter

ν = kinematic viscosity

ρ = density

μ = dynamic viscosity

For a laminar flow to occur, the viscous forces must be large enough to suppress flow fluctuations and to keep the fluid orderly.

For flow in a circular pipe (White, 2017);

Laminar flow: $Re \leq 2300$,

Transitional flow: $2300 \leq Re \leq 4000$,

Turbulent flow: $Re \geq 4000$.

The typical velocity profile for fully-developed flow is parabolic in laminar flow and flatter or fuller in turbulent flow (White, 2017). More analysis on types of fluid flow on heat exchangers are carried out on a pin fin also considered as a circular cylinder.

In spite of extensive experimental and numerical studies over the past century, flow around a circular cylinder still remains a challenging problem in fluid mechanics. Intensive investigations continue even today to understand the complex unsteady dynamics of the cylinder in wake flow. Cross-flow normal to the axis of a stationary circular cylinder and the associated problems of heat and mass transport are encountered in a wide variety of engineering applications. Both experimental measurements and numerical computations have confirmed the onset of instability of the wake flow behind a cylinder beyond a critical Reynolds number, leading finally to a kind of periodic flow identified by definite frequencies, known in the literature a is the Von Karman vortex street (Shao, 2007). In the case of laminar flow past cylinders with regular polygonal cross-section, the flow usually separates at one or more sharp corners of the cross-section geometry itself, forming a system of vortices in the wake on either side of the mid symmetry plane. On the other hand, for a circular cylinder, where the point of flow separation is decided by the nature of the upstream boundary layer, the physics of the flow is much more complex than what its relatively simple shape might suggest (Zdravkovich, 1997).

As the flow Reynolds number based on the free stream velocity, cylinder diameter and kinematic viscosity of the fluid changes from a creeping laminar flow value of the order of 0.1 to a turbulent

flow with a Reynolds number of a million or even higher, a variety of physical complexities start taking place. Steady laminar flow exists at Reynolds number between 5 and 40 with a pair of symmetric counter-rotating vortices formed behind the cylinder (Williamson, 1996). Shao (2007) also stated that between a Reynolds number of 190 and 260, wakes of two dimensional cylinders are observed to become susceptible to a primary instability mechanism which leads to the amplification of three-dimensional disturbances and eventually to the development of strong stream-wise oriented vortical structures. These three-dimensional disturbances alter the structure and evolution of the wake vortices and as a result, even at low Reynolds number, two-dimensional simulations often fail to accurately predict even gross flow quantities like mean drag coefficient and root mean square (RMS) of the lift fluctuation.

Zdravkovich (1997) compiled almost all the experimental, analytical and numerical simulation data available since 1938 on flow past cylinders and systematically classified this challenging flow phenomenon into five different flow regimes based on the Reynolds number. The computation is restricted only to the first few regimes designated by Zdravkovich as creeping laminar state (L1) of flow ($0 < Re < 4$), laminar flow (L2) with steady separation ($4 < Re < 48$) forming a symmetric contra-rotating pair of vortices in the near wake, laminar flow (L3) with periodic vortex shedding ($48 < Re < 180$) and finally part of the transition-in-wake (TrW) regime ($180 < Re < 400$) when the three-dimensional instabilities lead to the formation of stream-wise vortex structure.

1.3 INTRODUCTION TO ANSYS FLUENT

Ansys Fluent is a fluid dynamics software package for modelling flow and other related physical phenomena, which offers unparalleled analysis capabilities. Fluent provides all the tools needed

to design and optimize new equipment and to troubleshoot existing installations. The versatile technology offers insight into how a product design will behave in the real world, all before a single prototype is built. The software provides accurate insight into a product's behaviour quickly and efficiently. The software is based on the finite volume method where its domain is discretised into a finite number of control volumes (ANSYS Fluent, 2011). General conservation (transport) equations for mass (continuity), momentum, energy, and species are solved on the set of the control volumes. Partial differential equations are discretized into a system of algebraic equations as shown in Equation 1.2:

$$\frac{\partial}{\partial t}\int_V \rho\emptyset\, dV + \oint_A \rho\emptyset V \cdot dA = \oint_A \Gamma_\phi \nabla\emptyset \cdot dA + \int_V S_\emptyset\, dV \tag{1.2}$$

Fluent further numerically solves all the algebraic equations to render the solution field. In short, the software takes the following steps: pre-analysis, geometry, mesh, physical setup, numerical solution, verification, and validation (Shujan, 2016).

To provide high productivity, the ANSYS Workbench platform directly couples with various CAD software packages and automatically extracts and meshes fluid volumes. In this work, Solid-Works and Space-Claim are the CAD software used to specify the compact heat exchanger fin design environment. This operation is performed via a small set of parameters such as conformal and non-conformal mesh. The yield is the high-quality meshes critical for both accurate and fast CFD simulations.

The Computational Fluid Dynamics (CFD) is known to be the solution methods used to numerically solve fluid mechanics equations to predict fluid flow, heat and mass transfer, chemical reactions and related phenomena. To predict these phenomena, CFD solves equations for

conservation of mass, Newton's second law (F = ma), conservation of energy, etc. This can provide following detailed information on the fluid flow behavior:

- Distribution of pressure, velocity, temperature, etc.
- Forces like lift, drag (external flows, aero, auto….etc.),
- Distribution of multiple phases (gas-liquid, gas-solid...etc.),
- Species composition (reactions, combustion, pollutants...etc.).

CFD is used in all stages of the engineering process including the following:

- Conceptual studies of new designs
- Detailed product development
- Optimization
- Troubleshooting
- Redesign

CFD analysis complements testing and experimentation by reducing total effort and cost required for experimentation and data acquisition. The Ansys CFD makes use of the schematic shown in Figure 1.3 with other tools.

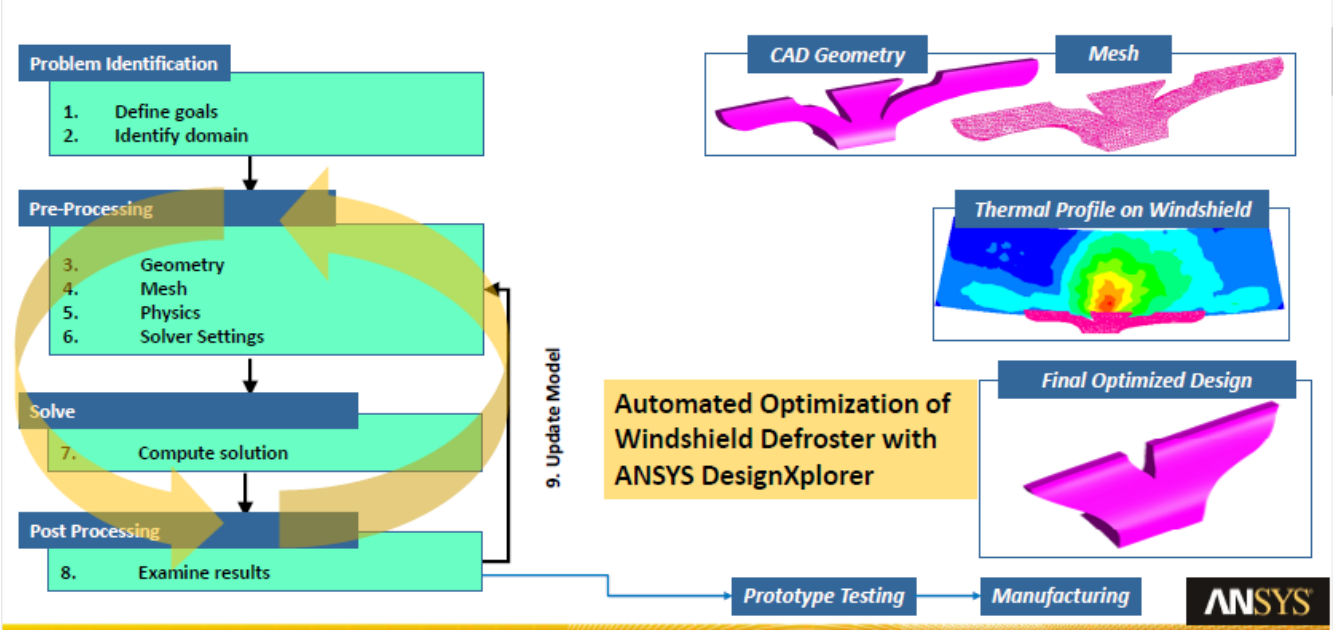

Figure 1.3: Ansys CFD flow chart (ANSYS, 2018).

1.4 CONTENTS OF DISSERTATION

In this work, computations are carried out over the Reynolds number range $0.1 < Re < 2600$, and subsequently compared with available measurement data and other computational results for steady-flow solutions. All the computations use an implicit pressure-based finite volume Navier-Stokes algorithm for time-accurate prediction of the flow. The whole flow domain covering the L1-TrW regimes has first been computed under the assumption of two-dimensional flow. Later, in order to understand the effect of the three-dimensional disturbances on the complex wake vortex dynamics, three-dimensional analysis have been carried out at five different Reynolds numbers covering Laminar and Transition-Wake regimes already reported in the literature by a few researchers (Williamson, 1996). The present computational results have compared to available measurement data and other computational results for the wake flow structures, the temporal evolution of drag coefficient, the variation of separation angle, stagnation pressure and base pressure behind the cylinder as the Reynolds number increases and also for the frequency and

amplitude of the fluctuating forces arising out of the phenomenon of vortex shedding in relevant flow regime. The contents of the remainder of the dissertation are described below.

Literature Review:

In Chapter 2, previous published work in this field is reviewed. It also includes the classification and categorization of compact heat exchanger. This is where discussion of various past works/experiment/research of pioneers in the field of compact heat exchangers and the advantages, limitations of the flow the heat exchanger and as well as their applications is presented.

Research Methods:

Chapter 3 describes the research methods used in this work. This includes defining a process of achieving the stated objectives and data analysis techniques. The methods involved in fulfilling these aims are simulation and experimental procedures. These procedures involve stating step-by-step the operational stages of some utilized packages.

Discussions of Results:

Chapter 4 contains information on the collection, arrangement and presentation of the data gathered. It includes the analysis of the data gathered, stating the effectiveness of the process. The analysis of the data will include volumetric rendering of pressure, velocity and heat transfer coefficient contours, and streamlines. The current results are compared to previous computational and experimental works.

Conclusions and Recommendations:

Chapter 5 presents a summary of activities, stating whether the aims and objectives are accomplished in the dissertation. It also includes the advantages and disadvantages of the design optimization process and its application in the industry. There is also a discussion of areas of improvement and future work based on the findings of this project.

Appendices:

This includes detailed results of the work completed.

CHAPTER TWO

LITERATURE REVIEW

2.1 INTRODUCTION

In connection with the practical demand for the development of high-performance heat exchangers, experimental studies have been made on the flow and heat transfer performance of offset-strip-fin type compact heat exchangers by London and Shah (1968) and Mochizuki and Yagi (1977). Related basic studies have also been carried out experimentally and theoretically for the two-dimensional heat transfer system with a staggered array of flat plates by Sparrow et al. (1977), Sparrow and Prakash (1980), Cur and Sparrow (1980), and Patankar and Prakash (1981). The present work is similar to utilizes the information of these studies and expands upon it in several ways.

2.2 COMPACT HEAT EXCHANGERS

Most plate fin heat exchangers (PFHE) consists of a block with alternating layers of extended surfaces as plate-fins. These layers are separated by parting sheets and restrained by side bars. A large heat transfer area, light-weight per unit volume, high thermal performance, possibility of heat exchange among several streams, and close temperature on channels are the advantages which make the PFHE one of the more popular types of heat exchangers (Khoshvaght-Aliabadi, 2014). Khoshvaght-Aliabadi (2014), further stated PFHEs employed a wide range of temperatures and pressures for gas-gas, gas-liquid, and multi-phase duties, such as cryogenics for separation and liquefaction of air (Coldbox system), production of petrochemicals and large refrigeration systems, and natural gas processing and liquefaction. To make the PFHEs as compact as possible in these

applications, the complex plate-fins (perforated, offset strip, louvered, wavy, vortex-generator, and pin), can replace the plain fins.

The general perception on the dimensions of the heat exchanger is determined by the coefficient of heat transfer of the fluids, which implies that low thermal resistance combined with an increase in heat flow is achieved either by increasing the mass turbulence or application of very thin fluid films (Szücs, 1962). The size of the fluid film will expand the path of the thermal energy through its conductance across the wall. These findings led to the evolution of the so-called laminar-flow heat exchangers. Szücs and Heller also made three assumptions to solve the thermodynamics problem posed in determining the dimensions of the PFHE. The thermodynamic questions raised involves the quantity of heat dissipated by the fluid to the fins and the provision of a fin base temperature that varies with the direction of flow and the temperature profile of the fluid at the outlet. The answers to the posed questions introduce the concept of the fin efficiency and its calculation. The assumptions made in the classical computation method are of considerable importance. These assumptions are as follows:

1. The flowing fluid temperature close to the fin remains constant. This assumption remains invalid because fluid temperature changes with the direction of flow.
2. The thermal conductance in the fins takes place only in the direction normal to flow. Due to high thermal conductivity of the material utilized, which leads to high temperature difference within the fins, also in the direction of flow. This temperature difference cannot be ignored and also rendered the assumption not useful.
3. The flow is at completely steady-state conditions and there is negligible conductivity of the fluid are generally assumed in the classical computation method.

Much research work has focused on heat transfer and flow pattern of PFHE. Kays and London (1984) listed performance parameters of 21 kinds of aviation aluminum serrated plate-fin structures with condensing steam heating the normal temperature air in wind tunnel experiments. There are several different correlations for heat transfer and pressure drop for offset strip fins heat exchangers.

PFHEs use either corrugated or embossed plates that are packed to form channel passages for flow (Raju, 2011). There are two types of plate heat exchangers. One is the plate-and-frame or gasketed plate heat exchanger and the other is a welded or brazed plate heat exchanger. The gasketed plate heat exchanger is designated to accommodate a mounted mechanical cleaning device. Hence, this type of exchanger is appropriate for situations requiring frequent cleaning, such as in food processing. One of the problems with the gasketed plate heat exchangers is the presence of gaskets, which limits operating temperatures and pressures.

The serrated fin is widely used in PFHE for its compactness of the surfaces, being characterized by large heat transfer area in per unit volume and substantial heat transfer enhancement due to the boundary layer restarting at the interrupted channels formed by fins (Xilong, 2015). However, there is an associated increase in a large pressure drop for the interrupted arrays. In recent years, research has been performed concerning the characteristics of PFHE, including analysis of heat transfer and flow pattern and the design of structure.

An increase in substantial heat transfer area was achieved by making finer corrugations in press-manufacturing of plates. The heat transfer area on a plate was 1.4 m^2 in 1965 and increased to 2.2

m^2 in 1975, while the overall heat transfer coefficient increased from 3,000 W/m^2C to 4,000 W/m^2C (Mori, 1980).

Norris et al. (1942) tried to determine the effects of fin thickness, fin length, and fin pitch on the heat transfer coefficient on offset strip fins. Manson (1950) made the first attempt developing predictive correlations, even though the database he employed consists of dissimilar geometries. Briggs (1961) determined the effects that fin pitch had on the thermal performance of offset rectangular- fin surfaces.

Wieting et al. (1975) went further to develop correlations, which are power law curve fits through data for 22 geometries. The correlations misrepresent the transition region, and only predict laminar and turbulent flows. The comprehensive Colburn factor *j* and friction factor *f* correlations for the offset strip fins were obtained by Kays and London (1984). Joshi et al. (1987) conducted an experiment which identified the transition flow from laminar flow and predicted analytical models to predict Colburn factor *j* and friction factor *f* factors, and re-evaluated the correlations of Wieting et al (1975). Mochizuki (1987) also conducted experiments to fit correlations, with the coefficients and exponents. Correlations of Colburn factor *j* and friction factor *f* factor for offset strip fins are complex, and it is difficult for them to predict Colburn factor *j* and friction factor *f* factor in the transition region.

Hou (1988) performed a series of thermal tests in an attempt to verify the extension of Kays and London (1984) air tests to fluids, using water and ethylene glycol, for which the Prandtl number ranges from 0.7 to 70. The test results indicated that the Colburn and friction factors of serrated

fin are different for different types of fluids within the same Reynolds number range, indicating a significant effect of Prandtl number (Hou, 1988). Tinaut (1992) proposed the correlations for heat transfer and flow characteristics for offset strip fin heat exchangers using water and oil as the working fluids. Polyalphaolefin and water was used by Hu (1995) to investigate the effect of Prandtl number on offset strip heat exchanger performance.

Bergles et al. (1995) further revised the Kay and London experimental data and proposed correlations for Colburn factor *j* and friction factor *f*, which can be used in the laminar, transition and turbulent flow regions. These correlations are very complex, and the rms error of the predict equations for Colburn factor *j* and friction factor *f* are $\pm$20%. The effect of fin space, fin height, fin thickness, fin length and flow length on the heat transfer and pressure drop characteristics in 16 offset strip fins was studied by Dong (2007).

The general correlations of Colburn *j*-factor and Fanning friction *f* factor are developed by regression analysis and F significance test, which can predict 95% and 90% of the experimental data within $\pm$10% (Junqi, 2007). Peng and Ling (2008, 2011) performed a series of experimental studies of flow over offset strip fins at low Reynolds number.

Most previous researchers have focused on the serrated fins structure and material. In those studies, the geometrical parameters of the fins were changed by adjusting the thickness t_f, the wavelength s_f, the length l_f, and the height h_f of the serrated fins. The fins were commonly made of steel, aluminum, aluminum alloy, copper, etc. The serrated fins have always offset a half distance of fin width; however, irregular offset distance may change the structural parameters

significantly. Manufacturing irregularities, such as burred edges, bonding imperfections, and separating plate roughness also influence the flow and heat transfer characteristics in actual heat exchanger cores (Bergles, 1995).

Bhowmik and Lee (2009) analyzed fluid flow and heat transfer characteristics of offset strip fins in the laminar, transition and turbulent regions by deriving the general correlations for the Fanning friction factor *f* and Colburn *j* factors. They found a general correlation for Fanning friction *f* and Chilton-Colburn factor *j* are:

$$f_{cor} = 10Re_{dh}^{-0.68} \tag{2.1}$$

$$j_{cor} = 0.489Re_{dh}^{-0.45} \tag{2.2}$$

Furthermore, Bhowmik and Lee (2009) studied the effects of Prandtl number (Pr) in the fluid flow of Reynolds number of 10 to 3500, which gave the appropriate performance criteria for Pr = 7 and Pr = 50 to be thermal-hydraulic performance factor (*JF)*, flow goodness factor *(j/f)*, and volume goodness factor ratio ($j/f^{1/3}$), respectively.

In a study by Zhu (2008), four basic channels of the PFHEs, namely the rectangular plain, strip offset, perforated, and wavy, were simulated in the laminar flow regime. The main focus of this study was the heat transfer behaviours in both the developing and the developed regions and the local Nusselt number variations. Correlations for the thermal entry length were also obtained.

Kim (2011) developed a new numerical correlation by investigating the thermal-flow characteristics of PFHE with offset-strip fins for various fin geometries and working fluids which can be applied to offset-strip fins with blockage ratios greater than 20%. Zeng (2012) analyzed heat transfer characteristics and pressure drop of iron air preheater unit while Seara (2013) did the same for a titanium brazed plate heat exchanger. These works found the correlations of gas flow performance (Nusselt Number, fin efficiency) for a range of Reynolds number, Re = 5,000 – 11,000.

Based on the analysis of numerical data by CFD techniques for offset strip fins, new correlations for the general prediction of Colburn factor *j* and friction factor *f* factors were developed by Yujie (2014). These result correlate of a variety of geometrical parameters with blockage ratio ranging of 10% - 60% (Yujie, 2014).

Ismail et al. (2010) prepared a review of thermal–hydraulic performances of compact offset strip plate-fin heat exchangers, which reflect the significant progress made in the field during the last two decades. It is worthy of note that multiple correlations are available for offset fins, and designers may be confused to choose the best one due to the larger deviations between the correlations and experimental results. These variations are more than 30% for *f* factor and more than 20% in the case of *j* factor with respect to Kays and London experimental data (1984).

The optimization of the configuration of serrated fin in PFHE with genetic algorithm combined with Kriging response surface method (RSM) by Wen (2016) provided a set of optimal solutions with the objectives of maximum of Colburn factor *j* factor and minimum of friction factor *f*,

implying that the total heat flow rate, total annual cost and number of entropy production units of PFHE were optimized with the specified mass-flow rate under given space by multi-objective genetic algorithm (MOGA).

The two factors that affect the maldistribution of fluid flow in a heat exchanger are categorized into two types: mechanical factors such as improper design of the header and distributor, manufacturing tolerances, and plate corrugations, and of working conditions or fluid properties (Mueller, 1988). In order to improve the flow distribution, a fluid cavity and two stage header structure was proposed (Jiao, 2003).

Wetter (1999) created a simulation model of an air – to - air plate heat exchanger that uses the effectiveness – number of transfer units (ε – NTU) method which calculates the convective heat transfer coefficient based on an empirical correlation with a fixed exponent of velocity. Using the ε – NTU relation, he obtained ratio of the product of convective heat transfer coefficient (h) and surface area (A_s) values of both air streams at the nominal operating point and at nominal conditions.

Nakonjeczny (2006) performed numerical modelling of an air-to-air PFHE. He used unsteady-flow equations that are discretized with a semi-discrete finite-element method were utilized. This method can lead to a longer computational time and may cause difficulties in achieving convergence.

There are two types of comparison methods for the second-law performance evaluation which involves evaluating the heat transfer enhancement of offset strip fins by combining heat transfer and hydraulic characteristics. Bejan (1980) proposed a method to use the augmentation entropy generation number (Ns,a) which is characterized by the comparison of total entropy generation in an augmented channel and that in a reference channel, and has been extensively applied to the plate fin-channel and various other enhanced devices (Chakraborty, 2011, Chen, 1998, Tagliafico, 1996, and Zimparov, 2001). The other method is the entropy generation distribution factor, proposed by Manglik (1994), that involves the comparison between the reduction of the entropy generation due to the heat transfer enhancement and the increase of the irreversibility due to the increase in pressure drop.

In different quasi-steady-state and a dynamic models of a counter-flow air-to-air heat exchanger, it was discovered that the effects of dehumidification and frost formation needs to be accounted for with the geometric data when also calculating the Reynolds number (Rose, 2008, Rammer, 2009). Likewise, a theoretical model was developed to predict frosting limits for cross-flow air-to-air heat exchangers, which needs geometric data for the calculation of the heat transfer coefficient (Liu, 2016).

It is also shown in the Modelica Buildings Library, an open source simulation library that the effects of the changing air flow rates and temperatures are negligible when simulating the air-to-air heat exchanger model fluid with constant effectiveness (Nouidui, 2012).

In the flow resistance calculation of the model in Modelica Buildings Library, the relationship between pressure drop Δp and mass flow rate $\dot{m}$ is quadratic, which is not consistent with the situation in PFHEs. Investigations show that the correlation of the friction factor f in different PFHEs can be generally written as $f = k_1 k_2 Re^N$ (Bergles, 1995), where $k_1, k_2, Re, and\ n$ of shown correlations coefficient 1, 2, Reynolds number and exponential constant, respectively.

Numerous experimental studies using air as working medium have been applied to research the heat transfer performance in PFHEs with serrated fins. In these experiments, the air was heated from two sides of cover plate. Moreover, most of experiments were performed with constant temperature heating, except the tests of Dubrovsky (1988), for which discrete constant power heating plates were used. Based on the experimental data, predictions of thermos-hydraulic characteristics of serrated fin arrays was achieved (Bergles, 1995).

Numerous numerical studies were conducted on offset strip heat exchangers to predict thermal-hydraulic characteristics and to determine the effects of fin thickness, fin height, fin length and fin pitch (Amano,1985, Patankar, 1977, Suzuki, 1985). They found out that shorter fin offset length yields better heat transfer performance. Moderate deterioration of the performance are caused by larger fin pitch and large fin thickness have no effect on thermal-hydraulic characteristics except for its use on thermal energy recovery from waste gas.

Losier, et al. (2007) determined the 3D effects of rounded fin edges and geometric parameters on an offset strip-fin heat exchanger's overall performance. Kim et al. (2011) established a numerical model of offset-strip fins for various fin geometries and working fluids. The flow and thermal

characteristics of offset-strip fins were investigated, and general correlations of the offset-strip fins were derived. Saad et al. (2011) presented a CFD model to investigate the phases and pressure drop distribution in offset strip fin units. They developed a correlation for single phase friction factor *f* in offset strip fin microchannels for laminar to turbulent flow of water and air and compared with 3D CFD simulations.

A major challenge in designing optimal multi-stream plate fin heat exchangers is the large number of combinations of standardized fin geometries for various fin categories and types to choose from, which adds discrete aspects to an already complicated design problem (Kays, 2012). Therefore, an appropriate fin selection method is important in the plate fin heat exchanger design. In the past, few methodologies considered all possible fin type combinations in the design procedure to guarantee the optimum solution.

Shah (1982) and Cowell (1990) analyzed individual fins in a variety of different ways: volume vs. power consumption, frontal area vs. power consumption, area goodness but when it comes to the actual design, the selection of another surface can have an effect on the overall performance of an exchanger. This implies that the performance of fins in combination is important if there is any degree of interaction between the two (Cowell, 1990).

Pau and Zhu (1999) proposed two new concepts, which are identical-fin concept and Z-Y graph to select optimum fin types. The identical fin indicates that the same fin type is employed for all streams in the early design stage while the Z-Y graph is time consuming and also ignores mix and match fin types and may not reach the minimum plate fin heat exchanger size.

Picon-Nunez, et al. (2002) proposed a new term ‘‘Volume Performance Index” by rearranging the heat balance equations and plotted a graph of VPI against Reynolds number to select appropriate fin types. The selection is based on the assumed Reynolds number relying on a time-consuming trial and error procedure neglecting the effect of imposed design constraints on fin selection.

Recently, the basic fin geometries were used as variables and integrated into a cross flow plate fin heat exchanger design model to optimize total weight and total heat transfer area respectively (Peng, 2008, Yousefia, 2012). Discrete fin geometry variables result in a very complicated mixed-integer nonlinear programming (MINLP) design problem. To solve these discrete variables, Yousefi et al. (2013), developed a proposed variant of harmony search algorithm for design optimization.

Guo, et al. (2014) used fin geometries as continuous variables in PFHE design optimization, with the final selected fin types to be the closest standardized fin types with the design methodologies putting into consideration, the effect of imposed design constraints on fin selection (with one common assumption of identical fin category). Only one fin category, such as plain fin or offset strip fin, is employed in the design procedure, ignoring the possibility of mix and match fin categories in plate fin heat exchanger design could lead to sub-optimal design solutions. Due to the complexity of the design problem for multi-stream plate fin heat exchangers, a major limitation of existing technology is the lack of a general design methodology that can consider mix and-match fin type selection and imposed constraints simultaneously to take advantage of different fin characteristics.

The heat transfer performance of offset strip fins is increased by a factor of about 5 over plain fins of similar geometry. This is because offset strip fins increase the heat transfer coefficient and heat transfer area through repeated growth and destruction of boundary layers and increase the effective surface area, while plain fins simply increase heat transfer area per volume. But the increase of heat transfer coefficient is at the expense of higher pressure drop for offset strip fins (Taylor, 1990). Without appreciably destructing layers and changing heat transfer area, the heat transfer characteristics of louvered fin and wavy fin lie between those of plain and offset strip fins, and their pressure drop performance ranks in between them as well.

The most significant variables of offset strip fin geometry are the fin thickness and strip length in the flow direction that leads to higher heat transfer coefficient and higher friction factors than plain fin geometries. This is enhanced by the interruption of the flow periodically, which does not only create fresh boundary layers but also generate greater viscous pressure drop due to higher friction factor as shown in cross sectional view show in Figure 2.1

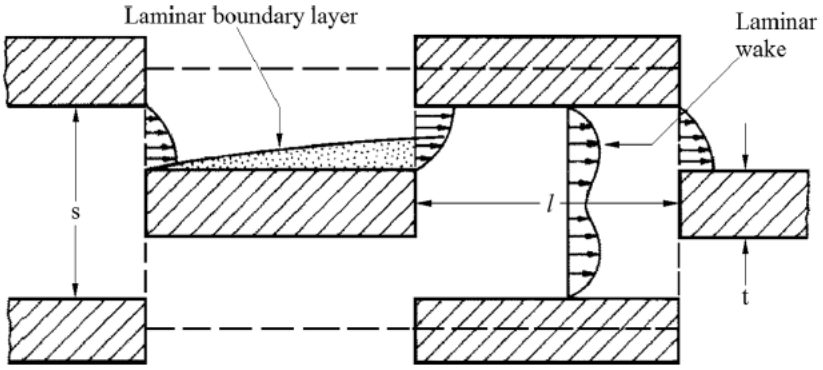

Figure 2.1: Flow patterns observed in visualization experiments (Joshi, 1987).

Pressure drop is an important reference factor in the fin selection method. Minimizing heat exchanger volume in the optimization design will prefer fin types with high heat transfer coefficient, such as offset strip fin, and give a smaller heat exchanger size. But the pressure drop may not be in the allowed range. If that is the case, the fin type must be switched to other fin types with lower pressure drop. Therefore, regarding different heat transfer and pressure drop performance, and if there is need for big pressure drop difference requirements for two sides, especially in multi-stream heat exchangers, mix-and-match fin types can provide a better design solution (Taylor, 1990).

To simplify the fin selection problem, Guo et al. (2014) recommended an identical fin category screening method, in which the typical fin geometries of different standardized fin categories and types, such as fin pitch, fin length, fin thickness and fin height, are considered as continuous variables. By employing continuous expressions of Fanning friction factor and Colburn factor which are functions of Reynolds number and basic fin geometry parameters and regressing some design parameters as a function of basic geometry parameters, the discrete optimization problem caused by standardized fin parts can be converted into a continuous problem to avoid solving the mixed integer nonlinear programming (MINLP) problem directly.

In terms of the objective function, Picon-Nenuz et al. (2002) took the plate fin heat exchanger volume rather than heat transfer area as the evaluation criterion of heat exchangers design. In practice, due to material and manufacture feasibility, capital costs of different fin categories are different. Moreover, due to porosity issues, the total weights of different fin categories per unit volume are different. Mix-and-match fin selection are considered in the design methodology,

minimizing the total capital cost is used as the objective function. Eight different fins were examined which differ from each other by their fin numbers per inch, type of flow section, fin height, distance between plates, flow length, fin thickness and the material used in the study. Due to diverse fin type used in their studies, Kays and London (1984) and London and Shah (1968) have developed a coding method that is stated in Table 2.1 which differentiate the fins from each other. An example of that coding might be given as the following:

$$\underset{1}{25}.\underset{2}{01}.\underset{3}{R(S)} - \underset{4}{0.201}/\underset{5}{0.200} - \underset{6}{1}/\underset{7}{9(O)} - \underset{8}{0.004}\underset{9}{(A1)} \tag{2.3}$$

The numbers given underneath the code stands for; number of fins per inch, type of fin flow cross section (R=rectangular, T=triangular, U=U shape), fin sandwich construction (SD=single-double, S=single, D=double, T=triple), fin height before brazing, fin height after brazing, uninterrupted fin length, type of surface (L = louvered, O = offset, P = plain, S = strip), fin metal thickness, fin material (Al = aluminium, SS = stainless steel, Ni = nickel, etc.) respectively.

Table 2.1: Explanation of codes (Latife, 2017).

Number	Explanation of code
1	Number of fins per inch
2	Type of fin flow cross-section
3	Fin sandwich construction
4	Fin height before brazing (inch)
5	Fin height after brazing (inch)
6	Uninterrupted fin length (inch)
7	Type of surface
8	Fin metal thickness (inch)
9	Fin material

Since experiments are the basis of the OSF heat exchanger research, it would be better to understand their terminology to distinct the varying geometries and structures.

Hyunkyu Moon, et al. (2021) designed, fabricated and tested an optimized tube-in-tube heat exchanger which had volumetric power density that was twenty times than current commercial tube-in tube heat exchangers. This heat exchanger was fabricated with the help of 3D printing technology using powdered AlSi10Mg. This is currently believed to be the future of compact heat exchangers.

2.3 VACUUM BRAZING WELDING

To be manufactured plate-fin heat exchangers are stacked, and the assemblies are placed into a vacuum-brazing furnace wherein the assembly is converted into an integral, solid structure. During the process, an Al–Mg–Si alloy coating on the parting sheets melts and bonds the Al alloy fins, parting sheets, and bars together to form a core block. The melting temperature of the brazing alloy is within 50°F (28°C) of the melting temperature of the base Al alloys. The process is a very precise and highly guarded process. Brazed Aluminium plate fins are used in low-temperature (cryogenic) gas processing services. Brazed Aluminium can also handle up to 10 fluids in a single exchanger "cold box". The cold box composed of alternating layers of corrugated fins and flat separator sheets called parting sheets.

Brazed Aluminium Heat Exchanger (BAHX) are at the heart of the cryogenic processes producing the industrial building blocks increasingly in demand throughout the world. The industrial gas industry requires BAHX to produce the pure components of nitrogen, oxygen and rare gases in highly efficient cryogenic processes. BAHX are incorporated into hydrocarbon processing

applications for the production of important basic products such as ethylene, propylene, hydrogen and natural gas, which all require cryogenic processing. Worldwide demand for natural gas, driven by its economic and environmental benefits versus other fossil fuels, is predicted to increase for the foreseeable future. BAHX plays a fundamental role in its purification and liquefaction and also enable the extraction of valuable by-products such as helium and natural gas liquids (NGL).

The matrix assembly is brazed in a vacuum furnace. The brazing process is highly complex and rigorously controlled to ensure a bond between each fin and corresponding plate. Even in a small heat exchanger that means millions of brazed joints. Each one is formed through capillary action as the brazing alloy on the surface of each plate melts during the high temperature operation and fuses to the parts in contact with it.

CHAPTER THREE

RESEARCH METHODS

3.0 INTRODUCTION

This chapter provides a detailed description of research method used in this work. Computational fluid dynamics is playing a vital role in solving problems in power engineering, aerospace applications, electronics, automobiles, cryogenics and air conditioning systems.

3.1 METHODOLOGY

In this section, the research methodology employed in this work is described. This method defines the mode and means of data collection and how results are analyzed. The methods used in this project involve numerical simulations. The research methods involve changing variables and studying how these variables ultimately impact the results. The numerical simulations are verified through comparison with previously-published experimental results. Once the numerical methodology is verified, many more simulations with varying data inputs can be run than is feasible with experimental work so that new designs can be proposed.

3.2 SIMULATION

Computational Fluid Dynamics (CFD) uses numerical methods and algorithms to solve and analyze fluid flow problems. CFD is used to predict internal or external fluid flow, heat transfer, mass transfer, combustion and chemical reactions by solving governing equations using a numerical process. These numerical models can in turn be easily used to predict complicated problems, which can save the time and cost of setting up experiments.

After the geometry has been created in the pre-processor stage, by either using the same CFD software or a CAD software, the geometry is then divided into small cells or elements where the flow variables are solved at the centers of these discrete cells. This process of dividing the physical part into smaller cells is known as a mesh generation in CFD process. The quality of the generated mesh has a direct impact on the computational speed, degree of convergence, and the accuracy of the numerical solution. These generated cells or grids come in different shapes depend on the flow condition, laminar or turbulent, external or internal flow, and the geometry structure. The three-dimensional cell shapes include a tetrahedron, triangular prism, quadrilateral pyramid, and hexahedron.

3.2.1 ANSYS MESHING

Ansys Meshing is a component of Ansys workbench which combines and builds on strengths of preprocessing offerings from Ansys. It is able to adapt and create meshes for different physics and solvers CFD (Fluent, CFX and POLYFLOW), Mechanical (Explicit dynamics and Implicit), and Electromagnetic which integrates directly with other workbench systems.

As shown in Figure 3.1, there are three basic types mesh elements; tetrahedral, hexahedral and polyhedral.

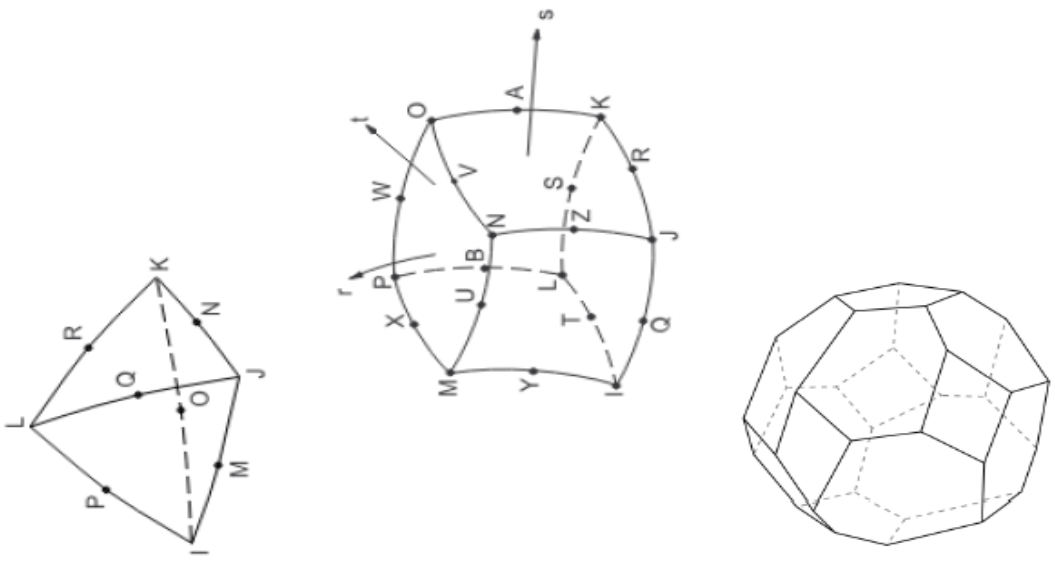

Figure 3.1: Schematics of the basic mesh elements: (a) tetrahedral, (b) hexahedral, and (c) polyhedral.

The tetrahedral and polyhedral elements are easier to mesh for more complex geometries than hexahedral elements. The tetrahedral elements can be easily converted to hexahedral elements if the mesh quality is good. Likewise, hexahedral elements produce faster solution with better accuracy than the tetrahedral and polyhedral.

It is noted that, mesh transitioning with a hexagonal mesh can be problematic because it involves re-ordering and deleting older meshes. Moreover, choosing the proper mesh element type will improve the mesh generation efficiency.

Good quality mesh implies that the mesh criteria are within the correct range. Such criteria include the orthogonal quality, element quality, skewness, warping factor, aspect ratio, Jacobean ratio, parallel deviation and maximum corner angle. These criteria show minimum, maximum, average and standard deviation. The impacts of a poor-quality mesh include convergence difficulties, poor description of the physics, and a diffuse solution. The criteria used for the simulation in this work

is orthogonal quality. Orthogonal quality is derived directly from the Fluent solver discretization which can be calculated on a face and cell as shown in Figure 3.2.

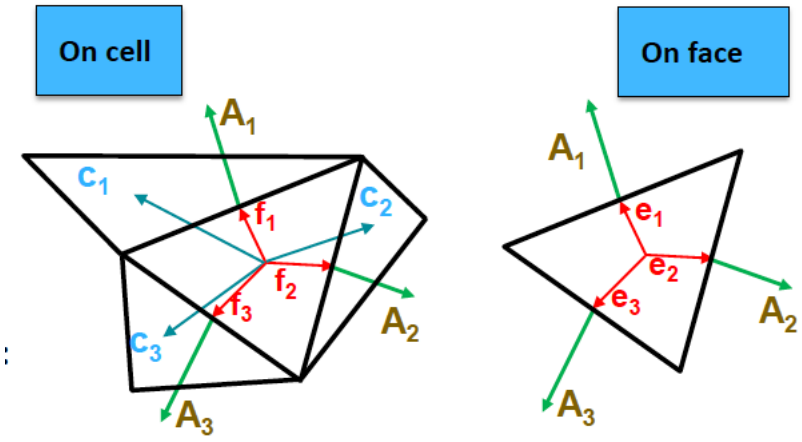

Figure 3.2: Schematic of the cell and face of the mesh.

On a cell, it is the minimum $= \frac{A_i f_i}{|\vec{A_i}||\vec{f_i}|} \frac{A_i c_i}{|\vec{A_i}||\vec{c_i}|}$ for each face i.

On the face, it is the minimum computed as = $\frac{A_i e_i}{|\vec{A_i}||\vec{e_i}|}$ for each edge l.

where, A_i is the face normal vector,

f_i is a vector from the centroid of the cell to the centroid of the face,

c_i is a vector from the centroid of the cell to the centroid adjacent cell,

e_i is the vector from the centroid of the face to the centroid of the edge.

It is often recommended that a good mesh should have a high orthogonal quality or low skewness on a scale of 0 to 1. However, these values may be different depending on the physics and the location of the cell. Table 3.1 shows the orthogonal quality mesh metrics spectrum.

Table 3.1: Orthogonal quality mesh metrics.

Unacceptable	Bad	Acceptable	Good	Very good	Excellent
0-0.001	0.001-0.14	0.15-0.20	0.20-0.69	0.70-0.95	0.95-1.00

3.2.2 ANSYS FLUENT

Ansys Fluent is a computer program for modelling fluid flow, heat transfer, and chemical reactions in complex geometries. Ansys Fluent is written in the C computer language and makes full use of the flexibility and power offered by that language. Consequently, true dynamic memory allocation, efficient data structures, and flexible solver control are all possible. It also utilises client/server architecture feature, which enables it to run as individual simultaneous processes on client desktop workstations and computer servers. This feature allows for efficient execution, interactive control, and complete flexibility between different types of machines or operating systems. Ansys Fluent provides complete mesh flexibility, including the ability to solve flow problems using unstructured meshes that can be generated about complex geometries with relative ease. Supported mesh types include 2D-triangular/quadrilateral, 3D-tetrahedral/hexahedral/pyramid/wedge/polyhedral, and mixed (hybrid) meshes. This also enables you to refine or coarsen your mesh based on the flow solution.

The Ansys Fluent serial solver manages file input and output, data storage, and flow field calculations using a single solver process on a single computer. Ansys Fluent also uses a utility called Cortex that manages Ansys Fluent user interface and basic graphical functions. Ansys Fluent's parallel solver enables one to compute a solution using multiple processes that may be executing on the same computer or on different computers in a network.

The Ansys Fluent solver manages file input and output, data storage, and flow field calculations. Processing involves an interaction between Ansys Fluent, a host process, and one or more compute-node processes. Ansys Fluent interacts with the host process and the compute node(s) using a utility called Cortex, which manages Ansys Fluent's user interface and basic graphical functions as shown in Figure 3.3. Ansys Fluent's serial solver uses a single compute node, whereas the parallel solver computes a solution using multiple compute nodes that may be executing on the same computer or on different computers in a network.

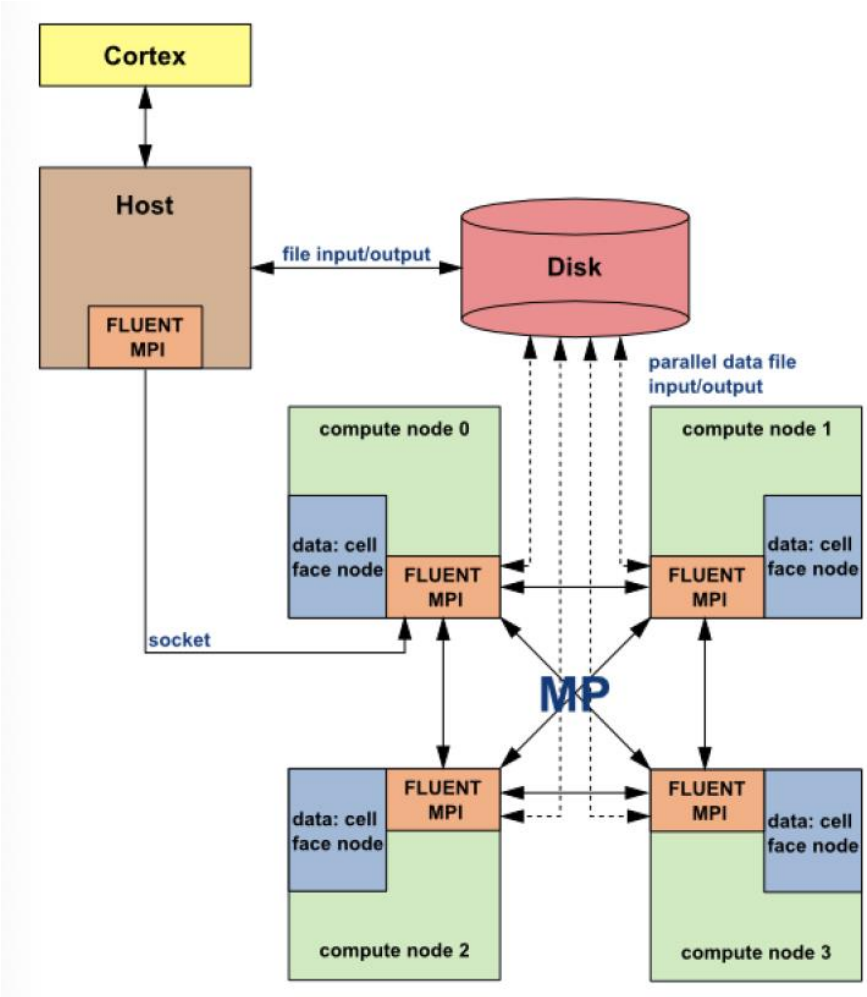

Figure 3.3: Ansys Fluent compute node (Ansys, 2018).

Ansys Fluent provides a standard database of materials and the ability to create a custom user–defined database. Material properties can be customized as function of temperature, mass-fraction or pressure (density). Use of other solution variable(s) requires a User–Defined Function (UDF).

Ansys Fluent actual needs the user to identify the cell and boundary zones. Here, the mesh consists of a large number of finite volumes or cells. Each cell is bounded by a number of faces. These faces are grouped into a number of face zones. Some of these faces are located on the boundaries of the model. The zones to which such faces belong are called boundary zones. Cell zone conditions are applied to all cell zones. Boundary conditions are applied to all boundary zones.

A fluid cell zone, or more simply, a fluid zone, is a group of cells for which all active equations are solved. Fluid material selection is also required. A solid zone is a group of cells for which only the heat conduction equation is solved. Flow equations are not solved. To define a problem that results in a unique solution, information on the dependent (flow) variables at the domain boundaries must be specified.

As the governing equations are differential and their solution requires integration, the boundary conditions are the mathematical equivalent of the constant of integration, the value of which is required to gain a unique solution and specify fluxes of mass, momentum, energy, etc. into the domain. It is noted that poorly defined boundary conditions can have a significant impact on the solution (i.e., solving "another" problem). Defining boundary conditions involves identifying types (e.g., inlets, walls and symmetry), identifying location, supplying required data depending on type, location and physical model. Choice depends on geometry, availability of data, and numerical considerations.

The Ansys Fluent chart gives a breakdown of the process and procedure as shown in Figure 3.4.

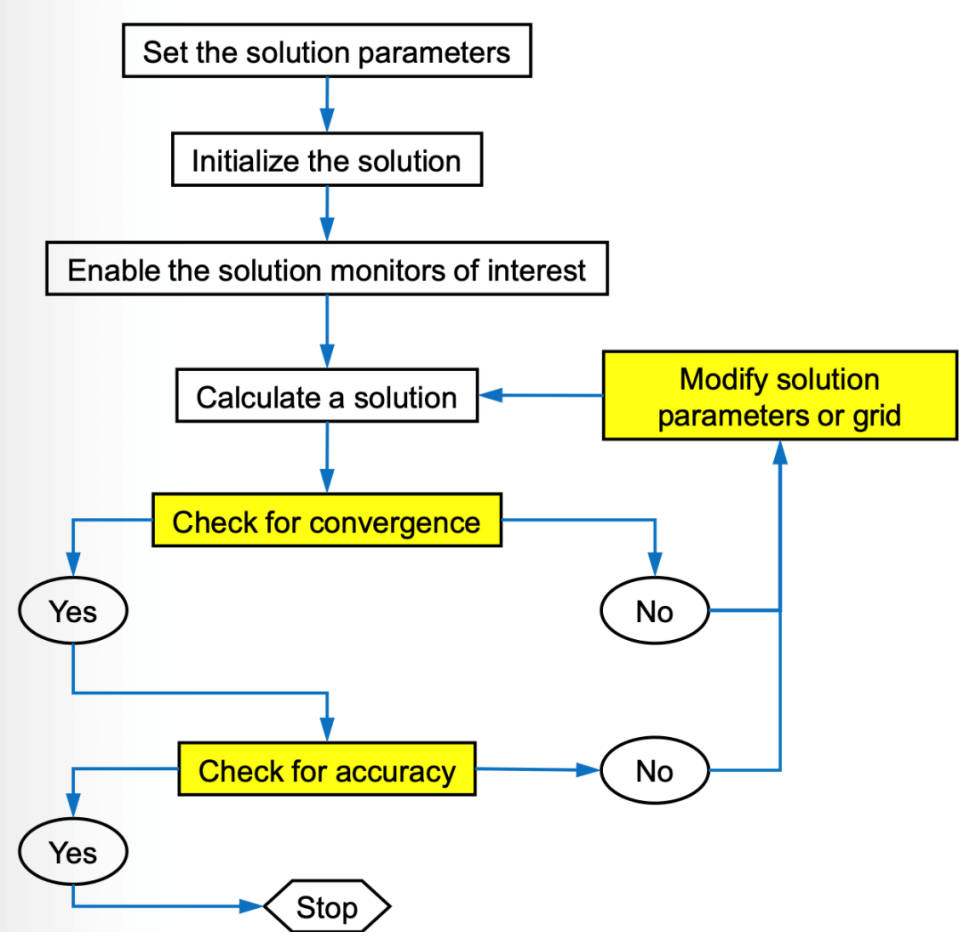

Figure 3.4: Fluent solution chart (Dimitrios, 2013).

Ansys Fluent Solution parameters are of two kinds of solvers, namely:

1. Pressure – based;
2. Density – based.

The pressure–based coupled solver is applicable for most flows and yields superior performance to the standard (segregated) pressure–based solver. This requires 1.5 – 2 times more memory than

the segregated solver. Fluent requires that all solution variables be initialized before starting iterations.

A realistic initial guess improves solution stability and accelerates convergence and, in some cases, a poor initial guess may cause the solver to fail during the first few iterations. There are three ways to initialize the flow field:

1. Standard initialization.
2. Hybrid initialization (solves potential equation).
3. Full Multigrid (FMG) initialization (solves Euler equations).

Under standard initialization, the user selects an inlet boundary under 'compute from' to automatically fill the initialization values with the values that are specified at the inlet boundary.

Hybrid initialization is the default initialization method. This provides a quick approximation of the flow field, by a collection of methods. It solves the Laplace equation to determine the velocity and pressure fields. All other variables, such as temperature, turbulence, species fractions, volume fractions, etc., will be automatically patched based on domain averaged values or a particular interpolation method.

Full Multigrid (FMG) Initialization can be used to create a better initialization of the flow field. FMG Initialization is useful for complex flow problems involving large pressure and velocity gradients on large meshes. FMG uses the Full Approximation Storage (FAS) Multigrid method to solve the flow problem on a sequence of coarser meshes. Euler equations are solved with first–order accuracy on the coarse–level meshes.

The initializations utilized in this thesis are Hybrid on the 6 inch x 3.5 inch, 4 inch x 3.5 inch, 3 inch x 3.5 inch, and FMG initialization on the 1 inch x 1 inch samples due to limitations of available resources.

The solver must perform enough iterations to achieve a converged solution. All discrete conservation equations (momentum, energy, etc.) are obeyed in all cells to a specified tolerance (Residual). The residual measures the imbalance of the current numerical solution and is related but not equal to the numerical error. Overall mass, momentum, energy, and scalar balances are achieved. Target quantities reach the following constant values (in the steady-state solver).

1. Integral (e.g., pressure drop),
2. Local (e.g., velocity at specified position).

Convergence is monitored using residual history. Generally, a decrease in residuals by three orders of magnitude can be a sign of convergence (but not necessarily). Scaled energy residual should decrease to 10^{-6} (for the pressure–based solver).

3.3.2 STARCCM+

A second CFD solver package, STAR-CCM+, was by Siemens, Berlin, Germany, also utilized in the research work. Below are the details of STAR-CCM+ CFD solver package.

3.3.2.1 STAR CCM+ MESH GENERATION

STAR CCM+ contains different types of meshing models for generating the volume mesh of the geometry, with the selection depending on the flow problem in order to assure the quality of the

generated mesh. With the aid of the STAR-CCM+ manual (Siemens, 2018) the major types of meshing models in STAR-CCM+ are described in the following sections.

Tetrahedral Mesh

The tetrahedral mesh model provides an efficient and simple solution for many complex mesh generation problems using the tetrahedral cell shape to build the mesh core that can produce the fastest mesh model for the computation process, and the one that uses the least amount of memory. However, only few applications are suggested for use of this mesh model.

Polyhedral Mesh

The polyhedral mesh model is easy, efficient to build, and requires approximately five times fewer cells compared to the tetrahedral mesh model. Moreover, it is more numerically stable, less diffusive, and more accurate than an equivalent tetrahedral mesh. The model uses an arbitrary polyhedral cell shape to build the core mesh, and it requires almost the same amount of surface preparation as the tetrahedral Mesh model.

Trimmed Mesh

The trimmed mesh provides a simple and efficient method for producing a high-quality mesh for both simple and complicated geometries, and recommended when surface quality of the geometry is not good enough to use a polyhedral mesh. It uses a trimmed hexahedral cell shape to build the core mesh, and has the ability to refine cells in a wake region, this model is ideal for use in external aerodynamic applications.

Thin Mesher

The thin mesher model is typically used to generate a prismatic layered volume mesh for thin areas or regions within the geometry so that the high-quality cells can adequately capture the solid material thickness.

Prism Layer Mesher

The prism layer mesher cells are situated next to the wall boundaries in order to accurately capture the near wall velocity profile and temperature profile in turbulent flow applications and also to predict the flow variables such as pressure drop, laminar and turbulent shear stresses, and turbulent viscosity. However, this is an optional model that is strongly recommended to be used in internal turbulent flow applications. The thickness of the prism layer and the number of the prism layers are the two properties required to quantify when the prism layer mesh model is selected. The thickness of the prism layers determines the height of these layers and it can be either a relative thickness to the base mesh size or an absolute thickness with a length unit. The number of the prism layers property, as the name suggests, sets the number of prism layers needed for a given volume mesh.

3.3.2.2 Fluid Physical Models

Subsequently, after the creation of the geometry and selecting the appropriate mesh model, the fluid physical models have to be chosen prior to specify the boundary conditions and running the simulation. Table 3.2 summarizes the main physical models available in STAR-CCM+ software.

Table 3.2: List of all fluid physical models available in STAR CCM+ (Siemens, 2019).

Category	Available Physical Models
Flow Characteristics	Inviscid, laminar, or turbulent
	Newtonian and Non-Newtonian viscosities
	Incompressible and compressible
	Multiphase mixtures
	Porous resistance
	Gravitational acceleration
	Passive scalars
Space	Axisymmetric
	Shell three dimensional
	Three dimensional
	Two dimensional
Time	Explicit unsteady
	Harmonic balance
	Implicit unsteady
	Steady
Material	Gas
	Liquid
	Solid
	Multi-component (gas, liquid, solid)
	Multi-phase
Flow	Coupled flow (gas, liquid)
	Segregated flow (gas, liquid)
	Viscous flow (liquid)
Equation of State	Constant density (gas, liquid)
	Polynomial density (gas, liquid)
	Ideal gas (gas)
	Real gas (gas)
	User defined (gas, liquid)
Turbulence Models	K-Epsilon turbulence
	K-Omega turbulence
	Reynolds stress turbulence
	Spalart-Allmaras turbulence
Other Optional Models	Segregated fluid temperature
	Segregated fluid enthalpy
	Mesh deformation
	Exact wall distance
	Cell quality remediation
	Turbulence suppression
	Two-layer all y+ wall treatment (k-epsilon model)
	All y+ wall treatment (k-omega model)

After setting the boundary conditions for the CFD problem, initial values, entered by the user for the mean inlet velocity or pressure, outlet velocity or pressure, and the turbulence parameters at the duct inlet and outlet. The CFD solver starts the solving process by varying and iterating the initial conditions of the flow and by using the entered inlet and outlet boundary conditions to find a numerical solution for the partial differential equations of the flow. As the software approaches a solution, the simulation converges. On the other hand, when a poor mesh quality is used or a wrong physical model is implemented, the software deviates away from the solution, and the

simulation in such cases diverges. The solution residuals are one of the most fundamental measures of convergence in CFD simulations as they directly evaluate the solution errors associated with the flow variables in each control volume. As a result, each control volume will have a residual value for each of the partial differential equations being solved and they are set at 1.0×10^{-6} under the stopping criteria option.

CHAPTER FOUR

DISCUSSION OF RESULTS

4.1 INTRODUCTION

In this chapter, the heat transfer characteristics and compressed air flow patterns from the computational simulations of the seven fin designs are presented and analyzed. *Compact Heat Exchangers* by Kays and London (1984) provides background information on some of the fins analyzed and experimental data for comparisons. Figure 4.1 shows the geometric configuration and terminology of the offset strip fins. The geometrical parameters of the offset fin include the height of fin (H), lance length of the fin (l), fin frequency (fins per inch, n), and fin thickness (t) (Yousefi, 2013).

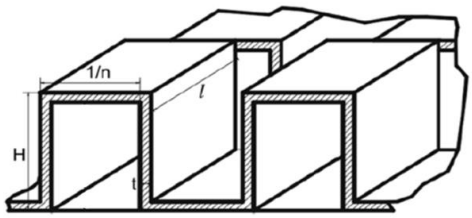

Figure 4.1 Schematic drawing of an offset fin (Yousefi, 2013).

Table 4.1 provides a detailed description of the fins studied. Some of other symbols used in Table 4.1 include the notch length (NL), hole spacing (B1), amplitude (a), and wavelength (λ). Of the seven fins analyzed, four are offset strip fins with similar configurations (606, 606notch, 161 and 161notch), while the remaining three fins are Perforated (519), Wavy (635) and a combination of the 606 and 635 fins which are 519, 635 and combination (606 & 635), respectively. The 606, 519, 635 fin designs originated from Kays and London (1984) compact heat exchanger text while the

606Notch and 161 fin designs are originated from our industry partner. The 161Notch and combination fin design was developed in the UWM Energy Conversion Efficiency Lab.

Table 4.1: Description of the seven fins studied.

FIN DESIGN	SECTIONED VIEW	INTERNAL DIMENSIONS (CM)
606	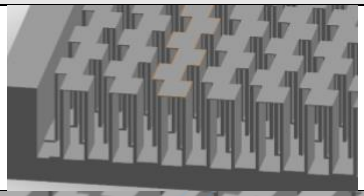	H = 0.953 t = 0.254 FPI = n = 13.95 l = 0.318
606NOTCH	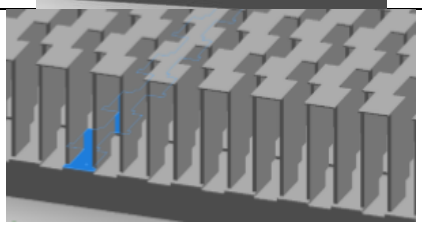	H = 0.953 t = 0.254 FPI = n = 13.95 l = 0.318 NL = 0.051
161	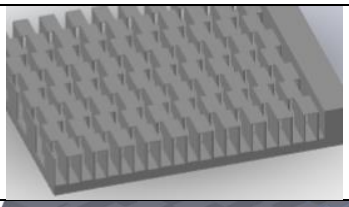	H = 0.965 t = 0.020 FPI = n = 18 l = 0.318
161NOTCH	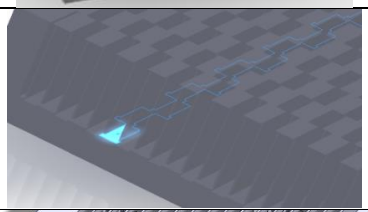	H = 0.965 t = 0.020 FPI = n = 18 l = 0.318 NL= 0.051
519	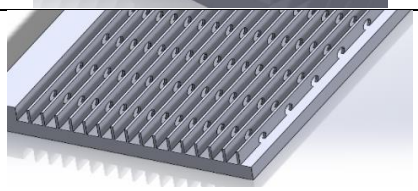	H = 0.965 t = 0.031 FPI = n = 12.95 D = 0.201 B1 = 81.28
635		H = 0.965 t = 0.015 FPI = n = 17.8 λ = 0.953 a = 0.20
Combination of 606 & 635	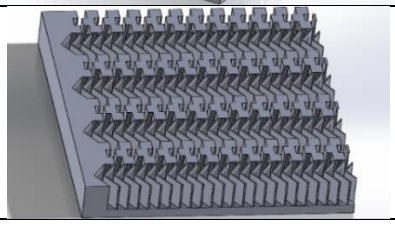	H = 0.953 t = 0.254 FPI = n = 13.95 l = 0.318

The offset strip fin 606, 606Notch, 161, and 161Notch were selected to predict the optimal performance between the original and notch models which were primary among the widely used highly effective fins. The objective of this research is to formulate an effective and accurate method to analyze compact heat exchanger fins designs and to identify fin configuration that have enhanced heat transfer capabilities with reduced pressure drop results. The results will be presented through plots of friction factor *f* and Chilton-Colburn factor *j* versus the Reynolds number *Re*.

The available data from Kays and London (1984) on compact heat exchanger fins utilized transient and turbulent flow. The flow being considered in this thesis is laminar flow because of its well-defined smooth streamlines that never cross one another and makes computational analysis more accurate. Ansys Fluent describes laminar flow as flows characterized by stable velocity fields while Siemen's STAR-CCM+ defines it as specifying the properties of the fluids/solid in the model which is an economic way of representing wall functions of boundary layers (Ansys, 2018), (Siemens, 2006).

4.2 VALIDATION OF SIMULATED RESULTS

Before the simulation results can be reliably used, it is necessary to verify the computational results through comparison with previously published data. The experimental data of Shah and London (1978) for uniform heat flux boundary conditions on all the four walls and the computational data using Ansys Fluent software of Dharaiya and Kandlikar (2012) for four and two-walls of uniform heat flux boundary conditions of a rectangular microchannel were used for comparison.

The reference work from Dharaiya and Kandlikar (2012) was further tested with Ansys Fluent 19.1 version and STAR-CCM+ 14.06.012-R8 Version to achieve the results listed in Table 4.2. In the STAR-CCM+ mesh set-up, Surface Remesher, Polyhedral Mesher and Prism Layer mesh were utilized. Equally, wrapping and tolerance level are amended to provide an adequate mesh in STAR-CCM+. However, these results could be fine-tuned to give matching values of the published Shah and London (1978) data by adjusting under-relaxation factors for both software programs. The under-relaxation factors are in the form of pressure, energy, Momentum, density, body forces, enthalpy, mass fraction etc.. These factors are always from 0 to 1 and can be in 1 to 14 decimals. These factors help to force convergence as discussed in Chapter 3.

Table 4.2 details the fully-developed laminar flow Nusselt number found by numerical simulations using Ansys Fluent and STAR-CCM+ as well as available published data for comparisons.

Table 4.2: Comparison of fully-developed Nusselt Number for Reynolds number of 100.

Aspect ratio $\alpha = 2b/2a$	**Heat Flux Application Boundary Conditions**	**Re**	**Nu (Shah and London, 1978)**	**Nu (Dharaiya and Kandlikar, 2012)**	**Nu (Ansys Fluent)**	**Nu (STAR-CCM+)**
0.5	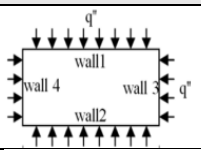	100	3.020	3.115	2.764	1.6807
0.5	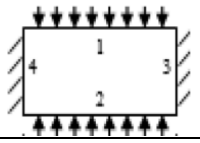	100	—	5.638	5.500	0.6859

Table 4.2, shows a 57% and 59.8% respectively percentage difference of the Nusselt number with the STAR-CCM+ software simulation results for the fully-developed laminar rectangular flow with the four-sided heat flux boundary condition with the Shah and London (1978) and Dharaiya

and Kandlikar (2012), respectively. There exists a 9% difference with the Ansys Fluent results with the experimental data of Shah and London (1978) and a 12% difference with the Dharaiya and Kandlikar (2012) data.

Changing the boundary conditions to a two-sided heat flux application, the STAR-CCM+ software yielded a percentage difference of 156.6% while the Ansys Fluent produced a 2.5% difference. From these results and the definition of laminar flow by STAR-CCM+ software package, it is demonstrated that STAR-CCM+ software is far less sensitive for laminar flows as compared to Ansys Fluent software. Thus, it was concluded to not use the STAR-CCM+ Software data for the comparisons in this thesis research. Since it would provide unreliable characterizations of the heat transfer and pressure drop for flow through the selected fin designs. Some STAR-CCM+ results are documented in the Appendix for comparison.

4.3 NUMERICAL SIMULATION RESULTS

The following are steps used in performing the CFD modelling:

1) Determine the smallest dimension among the length, width, height and thickness of the internal dimensions of the fin in order to determine the best mesh size for the fin.
2) Create the volume within the fin and form adequate contacts within the individual fins.
3) Create the heating pads/element around the suspected/required heated area for STAR-CCM+.
4) Perform the mesh creation (starting with a larger mesh number to a smaller one) with Ansys meshing and STAR-CCM+.
5) Setup the simulation within Ansys Fluent and STAR-CCM+.

6) Analyze and visualize the result.

This process was explained in more detail in Chapter 3. Analysis and visualization of the results are aided with the use of Word/Text file, plots/graphs and contour plots. Creation of the volume within the fin was done with Ansys Space Claim (a modelling software) and forming proper contacts within the array of fins was done when the CAD-volume file was imported into Ansys Meshing. It is important to note that not all of the fin arrays require contact-amendment (this is the amendment between each interlinking parts). The only design that required individual fin contact amendment before proceeding to meshing are the 635 fins.

The external dimensions of the fins are listed in Table 4.3. Here, the simulated fins are meshed, solved, and analyzed as a whole.

Table 4.3: External dimensions of simulated fins.

FIN DESIGN	EXTERNAL DIMENSIONS (cm)		
	L	W	H
606	5.08	8.89	1.60
606NOTCH	5.08	8.89	1.60
161	5.08	8.89	1.60
161NOTCH	5.08	8.89	1.60
519	5.08	8.89	1.60
635	5.08	8.89	1.60
Combination (606 & 635)	5.08	8.89	1.60

All seven fin designs were simulated have external dimensions of 5.08 cm x 8.89 cm. The meshing was done with non-conformal and polyhedral meshes with mesh size of 1×10^{-4} m and varied mesh size for the varied different samples, respectively.

In the Ansys Fluent mesh set-up, the non-conformal tetrahedral meshes are converted to polyhedral mesh with its quality being improved to an average of 0.7 which is under the good orthogonal quality range as discussed in Section 3.2.1.

The fluid used in this study is compressed air with properties listed in Table 4.4. The fin material used is aluminium with properties at standard state conditions of 25^{o}C listed in Table 4.5. With Ansys Fluent physics set-up, the option of solid Aluminum was employed.

Table 4.4: Properties of compressed air at standard conditions.

PROPERTIES	ANSYS FLUENT VALUES
density (ρ)	1.225 $\frac{kg}{m^3}$
specific heat capacity (c_p)	1006.43 $\frac{J}{kg \cdot K}$
thermal conductivity (k)	0.0242 $\frac{W}{m \cdot K}$
kinematic viscosity (v)	1.7894 x 10^{-05} $\frac{kg}{m \cdot s}$

Table 4.5: Properties of Aluminum at standard conditions.

PROPERTIES OF FIN MATERIAL (ALUMINIUM)	ANSYS FLUENT VALUES
density (ρ)	2719 $\frac{kg}{m^3}$
specific heat capacity (c_p)	871 $\frac{J}{kg \cdot K}$
thermal conductivity (k)	202.4 $\frac{W}{m \cdot K}$

Under the Ansys Fluent simulation, the flow was set to be laminar, steady, pressured-coupled and energy-coupled. The convergence criteria were set at 1 x 10^{-6} for all the residuals. After approximately 20,000 iterations, the flow converged. Each simulation took approximately 72 hours to run. Plots of the results are also provided in Figures 4.2 - 4.13. STAR-CCM+ simulation

data is not used for comparison, but is documented in the Appendix in Tables A.1 to A.20. The results in Tables A.1 to A.20 in the Appendix are derived from the equations below which was utilized by the Ansys Fluent software:

$$\text{hydraulic diameter} = D_h = \frac{2(h-t)(\frac{1}{n}-t)}{(h-2t+\frac{1}{n})} \tag{4.1}$$

$$\text{mass flowrate} = \dot{m} = \rho \cdot V \cdot A_c \tag{4.2}$$

$$\text{Reynolds number} = Re = \frac{\rho \cdot V \cdot D_h}{\mu} \tag{4.3}$$

$$\text{friction number} = f = \frac{8 \cdot \tau}{\rho \cdot V^2} \tag{4.4}$$

$$\text{pressure drop} = \Delta p = f \cdot \frac{\rho \cdot V^2 \cdot L}{2\ D_h} \tag{4.5}$$

$$\text{Chilton-Colburn factor} = j = St \cdot Pr^{\frac{2}{3}} \tag{4.6}$$

4.4 FRICTION FACTOR RESULTS

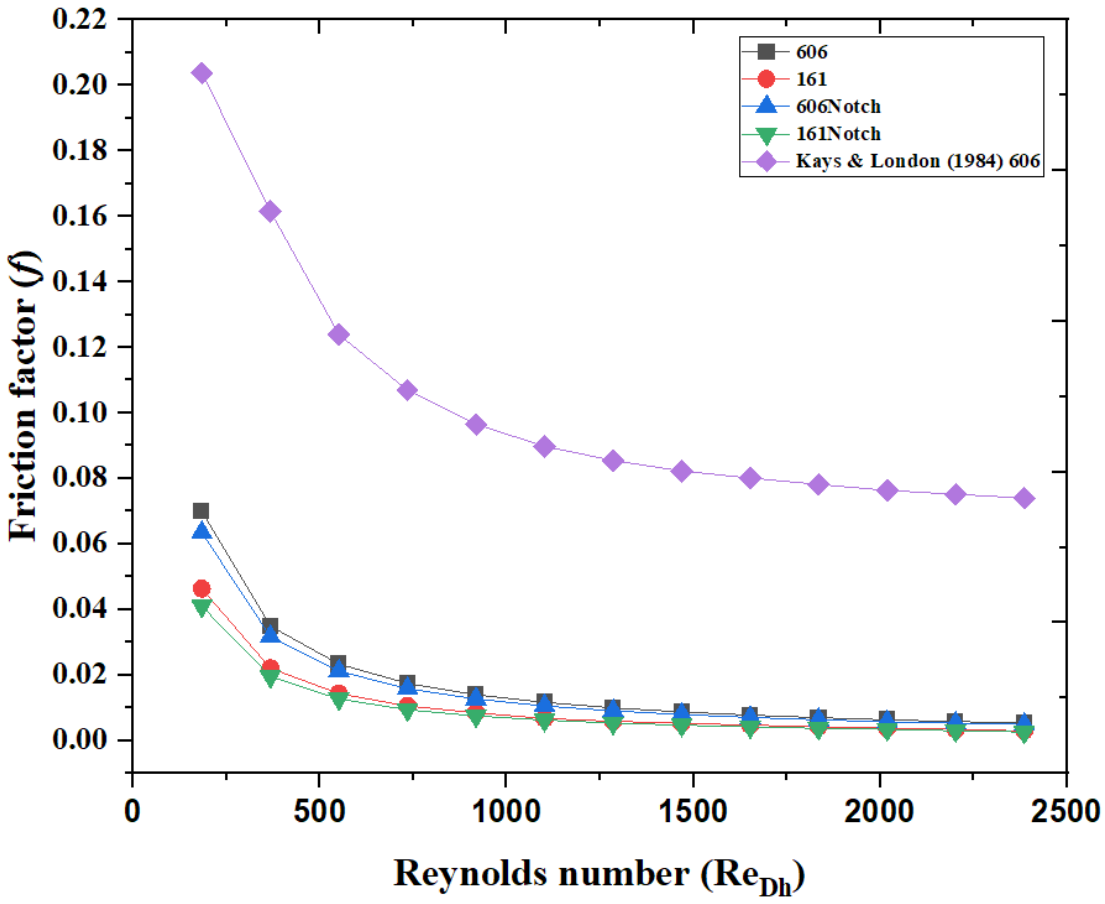

Figure 4.2: Friction factor (*f*) comparison for the 606, 161, 606Notch, 161Notch, fin designs data of Kays & London (1984).

Figure 4.2 is a comparison of the friction factor *f* versus Reynolds number of the 606, 161, 606Notch, 161Notch fin designs with the data of Kays and London (1984) 606 fin design. The comparison shows the Kays and London (1984) 606 data exhibits a higher friction factor *f* than 606 followed by the 606Notch, the simulations of 161Notch results are lower than those of the 161. As expected, the numerical simulations predict the friction factor *f* decreases as Reynolds number increases over the laminar flow range.

The 606, 606Notch, 161 and 161Notch fin design have an average friction factor percentage difference of 142.90%,147.5%, 162.3%, and 166.6% respectively with the Kays and London (1984) data. It is hypothesized that this difference in friction factor values is due to brazing and bending of the fin edges and the joining/welding of the fins.

Based on friction factor performance, the 161Notch performed best out of the four offset fin designs. Such a reduction in friction factor directly relates to a reduced pressure drop. The purpose of the Notch in the fin design is to allow better flow, a reduction in friction leading to reduced pressure drop. Hence as expected we see lower friction factor *f*. The difference in the 606 Notch and 161Notch are between the different fin internal dimension.

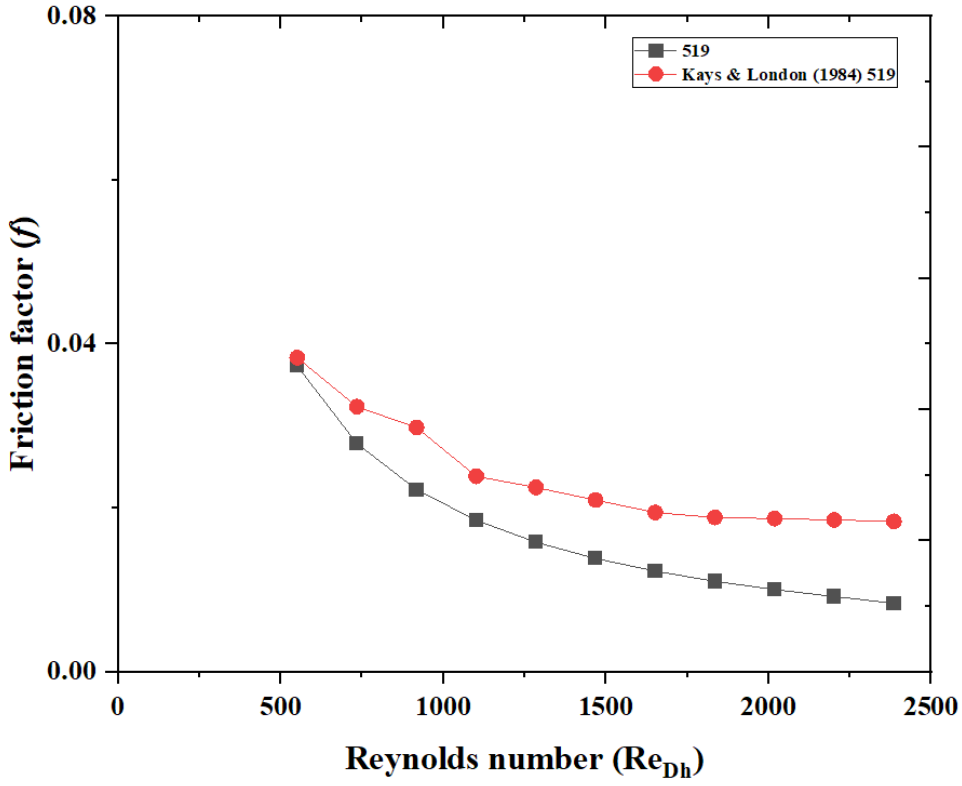

Figure 4.3: Friction Factor (*f*) comparison of the 519 fin design with the Kays and London (1984) 519 data.

Figure 4.3 is a comparison of the friction factor *f* of the 519 fin design with the Kays and London (1984) 519 data. The comparison shows the Kays and London (1984) 519 data exhibits higher friction factor *f* than the 519 simulation results for Reynolds number greater than 500. The 519, simulation results are very close to the experimental data except at the lowest Reynolds numbers. The 519 fin results have an average friction factor difference of 33.5%, with the Kays and London (1984) 519 data for Reynolds number greater than 500. As expected, the friction factor *f* decreases as Reynolds number increases over the laminar flow range.

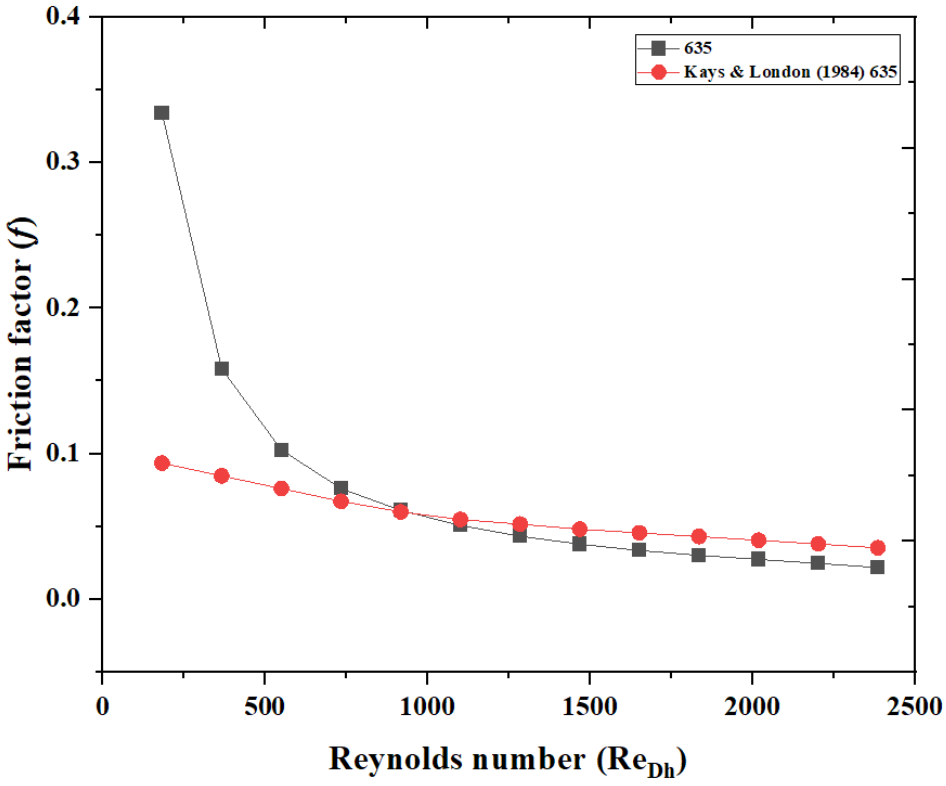

Figure 4.4: Friction Factor (*f*) comparison for the 635 with Kays and London (1984) 635 data.

Figure 4.4 is a comparison of the friction factor *f* versus Reynolds number fin design of the 635 fin design with the Kays and London (1984) 635 data. The comparison shows the 635 data nearly matches the kays and London (1989) data for Reynolds number greater than 750. Both results demonstrate the expected friction factor *f* decreases as Reynolds number increases over the laminar flow range.

The 635 simulation result have an average friction factor difference of 30.1%, with the Kays & London 635 (1984) data. Figure 4.6 also demonstrates the reliability of the Ansys Fluent simulation results.

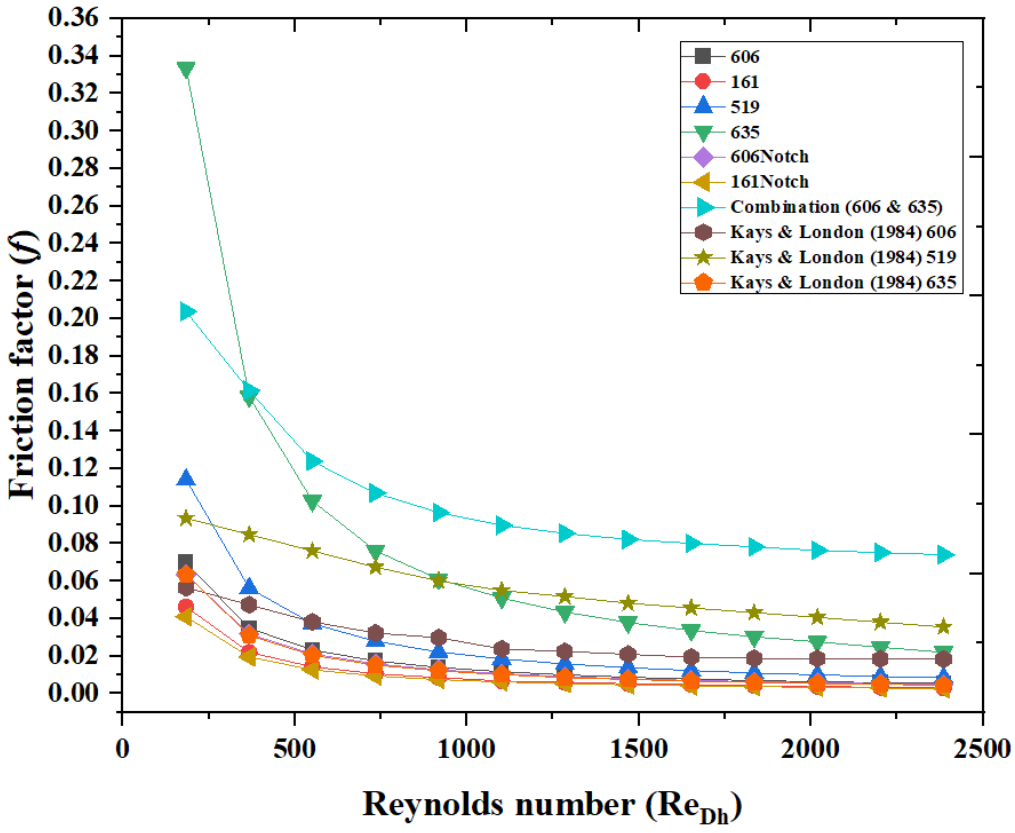

Figure 4.5: Friction Factor (*f*) comparison for the 606, 161, 519, 635, 606Notch, 161Notch, Combination (606 & 635) fins designs with Kays and London (1984) data.

Figure 4.5 is a comprehensive comparison of the friction factor *f* versus Reynolds number Re of the 606, 161, 519, 635, 606Notch, 161Notch, Combination (606 & 635) fin designs with the Kays and London (1984) 606, 519 and 635 data. The comparison shows the Kays and London (1984) 606 and 635 data exhibit the largest friction factors over the range of Reynolds numbers tested, while the 606, 161, 519, 606Notch, and 161Notch fin designs yield consistent lower values. As expected, we see the friction factor decreases as the Reynolds number increase for the data.

The 161Notch fin performed the best as compared to the other fin design due to the notch creating a free-flow environment outside a reduced pressure drop.

4.5 CHILTON-COLBURN FACTOR RESULTS (HEAT TRANSFER RESULTS)

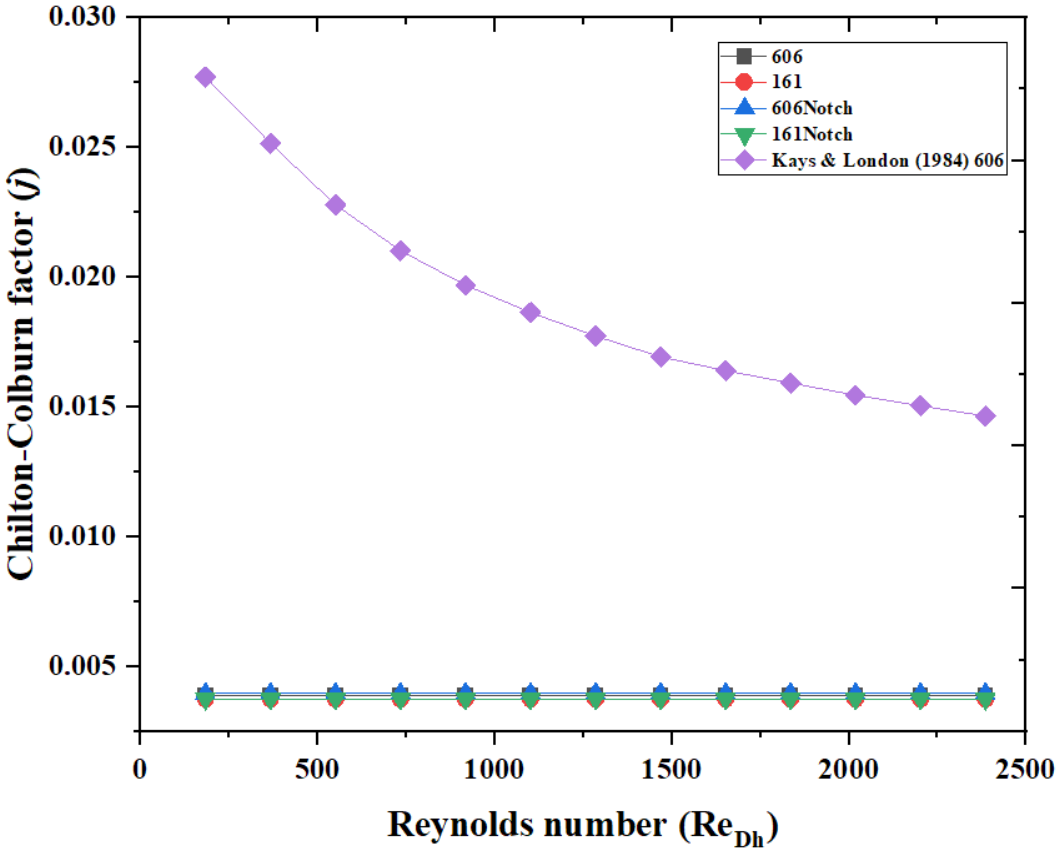

Figure 4.6: Chilton-Colburn Factor (*j*) comparison for the 606, 161, 606Notch, 161Notch fin design with data of Kays and London 606 (1984).

Figure 4.6 is a comparison of Chilton-Colburn factor *j* for the 606, 161, 606Notch and 161notch fin designs with the data of Kays and London (1984) 606. For the 606 fin design the highest is the Kays and London (1984) 606 fin design data. While the 606Notch, 606, 161,161Notch data are almost equivalent and constant. As shown, the Kays and London (1984) 606 data decreases as Reynolds number increases unlike the 606Notch, 606, 161 and 161Notch which are overlapping and unchanging as the Reynolds number increases as speculated. It generates such continuity for

the four fin designs noted that there is a slight increase in the heat transfer rate of the overlapping 606Notch, 606, 161 and 161Notch fin designs. This overlap is a result of the close resemblances of the 606 and 161 designs.

The 606Notch, 606, 161Notch and 161 fin designs have a heat transfer rate average percentage difference of 134.1%, 132.3% ,131% and 120.1%, respectively with the Kays and London (1984) 606 data. It is assumed the 161 fin design performed better because of its larger pitch and smaller thickness. These small differences in Ansys Fluent simulated results for Chilton-Colburn factor *j* suggests the sensitivity of the software to laminar flow.

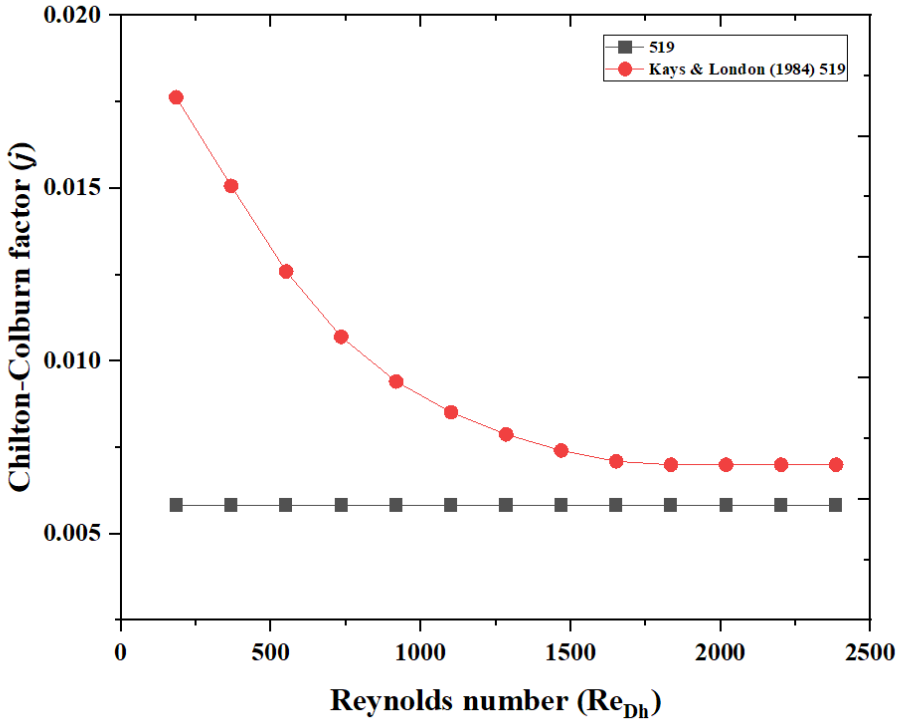

Figure 4.7: Chilton-Colburn Factor (*j*) comparison of the 519 fin design with Kays and London (1984) 519 data.

Figure 4.7 is a comparison of Chilton-Colburn factor *j* versus Reynolds number of the 519 fin design with the Kays and London (1984) 519 data. The numerical simulation results for the 519 fin design shows a lower value of heat transfer rate than the Kays and London (1984) 519 experimental data, over the range of Reynolds number tested. As expected, the heat transfer of the Kays and London (1984) 519 data decreases as Reynolds number increases unlike the 519 numerical simulations that show minimal differences over the Reynolds numbers tested.

The 519 data has an average difference in value of 50.5% compared to the Kays and London (1984) 519 data.

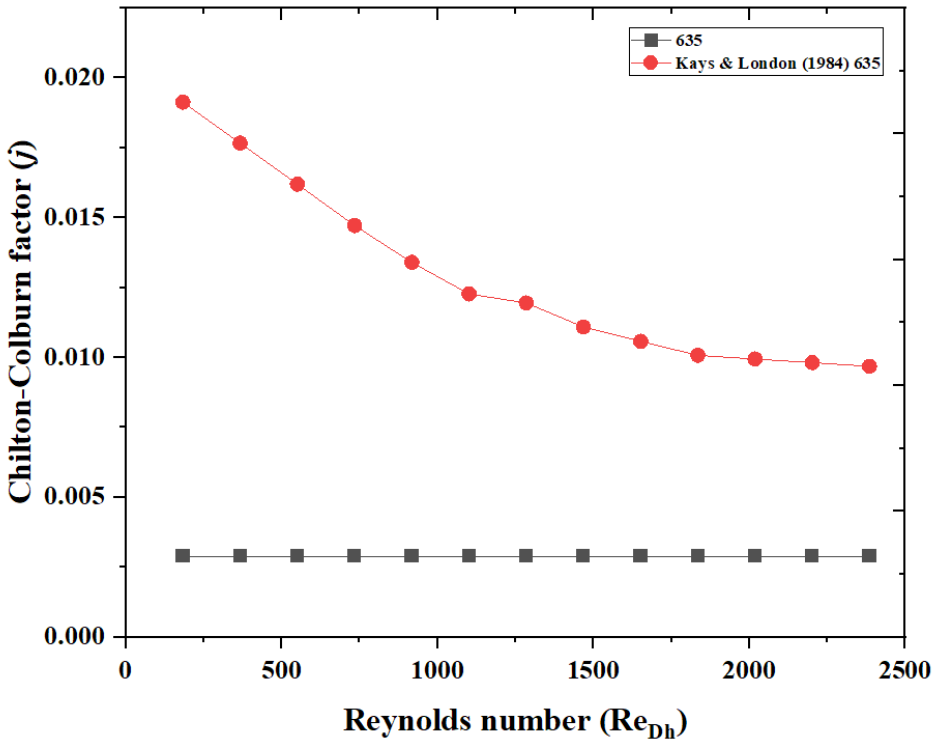

Figure 4.8: Chilton-Colburn Factor (j) comparison for the 635 fin design with Kays and London (1984) 635 data.

Figure 4.8 is a comparison of the Chilton-Colburn factor, *j* of the 635 fin design with the Kays and London (1984) 635 data. The Kays and London (1984) 635 data shows a higher heat transfer rate as compared to the numerical simulation data. The heat transfer of the Kays and London (1984) 635 data decreases as Reynolds number increases, while 635 numerical simulations are rather constant over the Reynolds number range. The unnoticeable increase in Chilton-Colburn factor *j* of the 635 stimulation with Reynolds number is a result of the laminar setting in the Ansys fluent program.

The 635 simulation result has heat transfer rate average difference of 130.3%; with the data of Kays and London 635 (1984) 635 data.

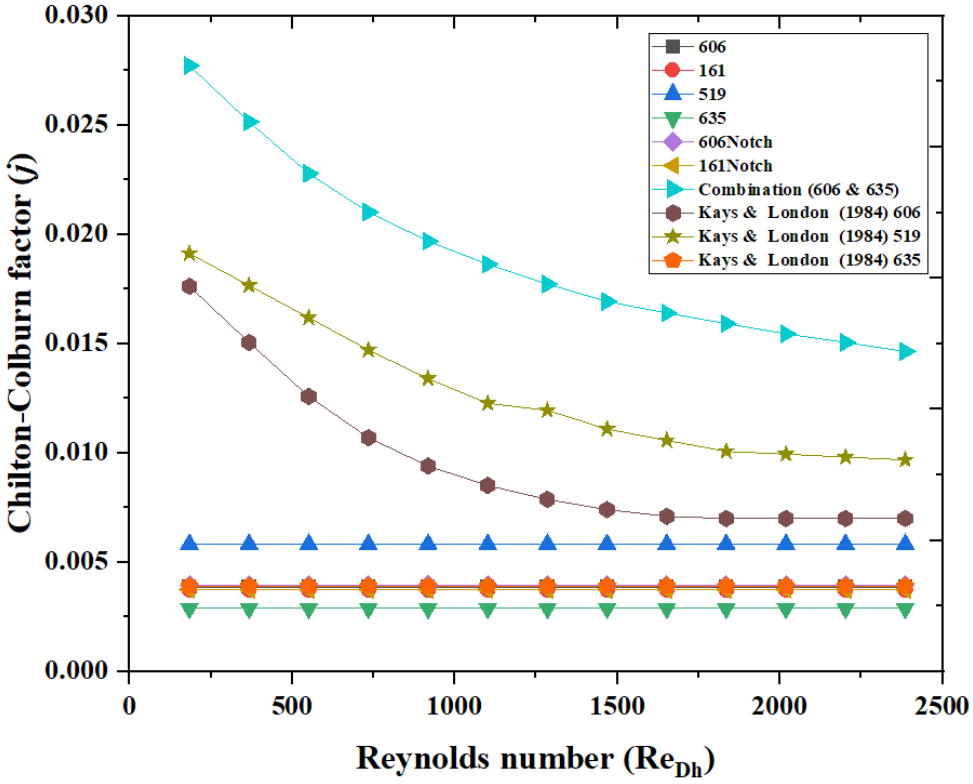

Figure 4.9: Chilton-Colburn Factor (*j*) comparison for the 606, 161, 519, 635, 606Notch, 161Notch and Combination (606 & 635) fin designs with Kays and London (1984) data.

Figure 4.9 is a comparison of Chilton-Colburn factor *j* versus Reynolds number of the 606, 161, 519, 635, 606Notch, 161Notch and Combination (606 & 635) with the Kays and London (1984) data.

The 519, Combination (606 & 635), 606, 606Notch, 161Notch, 161, and the 635 data shows a slight increase in heat transfer rate with increase in with increase in Reynolds numbers. The 519 fin design performed best of the seven fins tested. There was an approximately 38 % increase as compared to 606Notch which is as a result of the 519 fin design's interconnecting holes that allows interaction of the fluid as it passes through each channel an average tube at the same time contributed to the increase.

4.6 MESH SIZE RESULTS

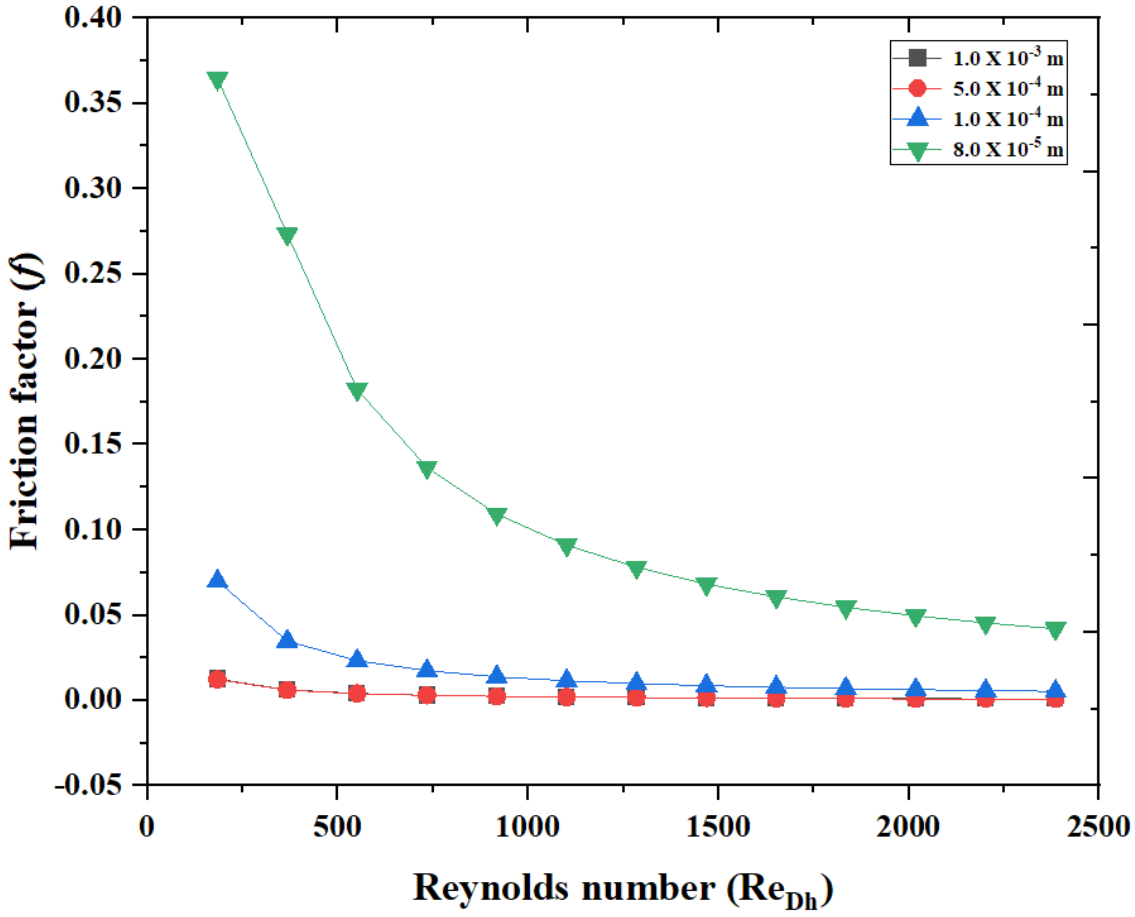

Figure 4.10: Friction Factor (f) comparison of different mesh sizes for the 606 fin design.

Figure 4.10 is a comparison of the results using different mesh sizes results for the friction factor *f* for the 606 fin design found using Ansys Fluent software. The size of the mesh utilized in the numerical simulations plays a very important role in obtaining accurate results. As expected, the 8.0 x 10^{-5} m mesh size provides the most accurate data. Here, we see the friction factor, *f* decreasing significantly as the Reynolds number increases. A 150 -190 % average decrease in the friction factor *f* is realized over the range of Reynolds number tested.

The comparison shows the 8.0×10^{-5} m, 1.0×10^{-4} m results exhibit higher friction factor *f* followed by 5.0×10^{-4} m and 1.0×10^{-3} m. The friction factor *f* decreases as Reynolds number increases over the laminar flow range. The 5.0×10^{-4} m and 1.0×10^{-3} m mesh size are quite overlapping due to large mesh size.

For the 606 fin design, it is clear that the analysis of the pressure design for the fin is poor as the mesh size is decreased. We also see that there is a minimal sensitivity in the friction factor for the three larger mesh size tested. These data show a 150 – 190% difference between these three large mesh sizes and the premium mesh size of 8×10^{-5} m.

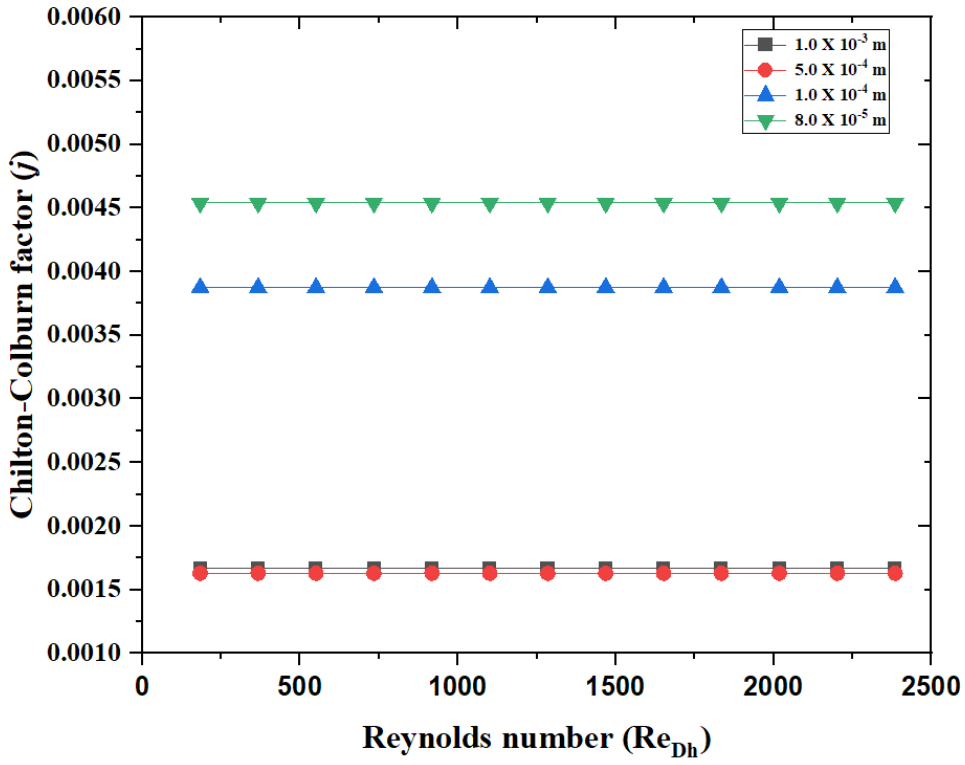

Figure 4.11: Chilton-Colburn Factor (*j*) comparison of different mesh sizes for the 606 fin design.

Figure 4.11 is a comparison of Chilton-Colburn factor *j*. The highest predicted heat transfer rate is with the mesh size of 8.0 x 10^{-5} m, followed by 1.0 x 10^{-4} m, 1.0 x 10^{-3} m while the 5.0 x 10^{-4} m simulation yields the lowest. As shown, the heat transfer of the different mesh size increases slightly with increase in Reynolds number. This inferred that the lower the mesh size, the better heat transfer application.

Again, we see the size of the mesh utilized during the numerical stimulations plays a very important role in determining accurate results. The smallest mesh size (8 x 10^{-5} m) provides the most accurate data. Here, we see that the Chilton-Colburn factor, *j* or heat transfer rate is relatively constant over the laminar flow range of Reynolds number tested. We also see that there exists an

average percentage difference of 16 – 93% between the three largest mesh sizes (1 x 10^{-3}, 5 x 10^{-4}, and 1 x 10^{-4} m) and the smallest mesh size (8 x 10^{-5} m) tested.

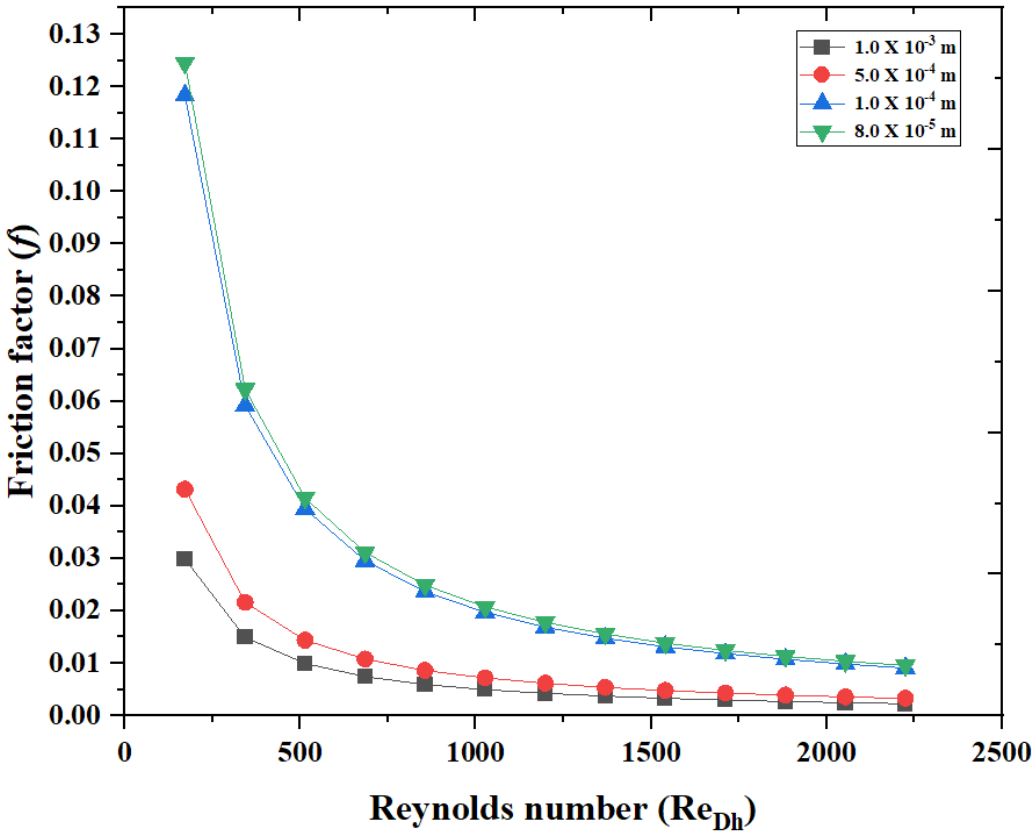

Figure 4.12: Friction Factor (*f*) comparison of different mesh sizes for the 519 fin design.

Figure 4.12 is a comparison of the different mesh size for friction factor *f* of the 519 fin design using Ansys Fluent. The two smaller mesh sizes showed considerable agreement over the laminar flow range of Reynolds number tested. As the mesh size increased, the average percentage difference between values of the friction factor for the two larger mesh sizes (1 x 10^{-3}, 5 x 10^{-4}, and 1 x 10^{-4} m) is 97 - 122% as compared to the smaller mesh sizes.

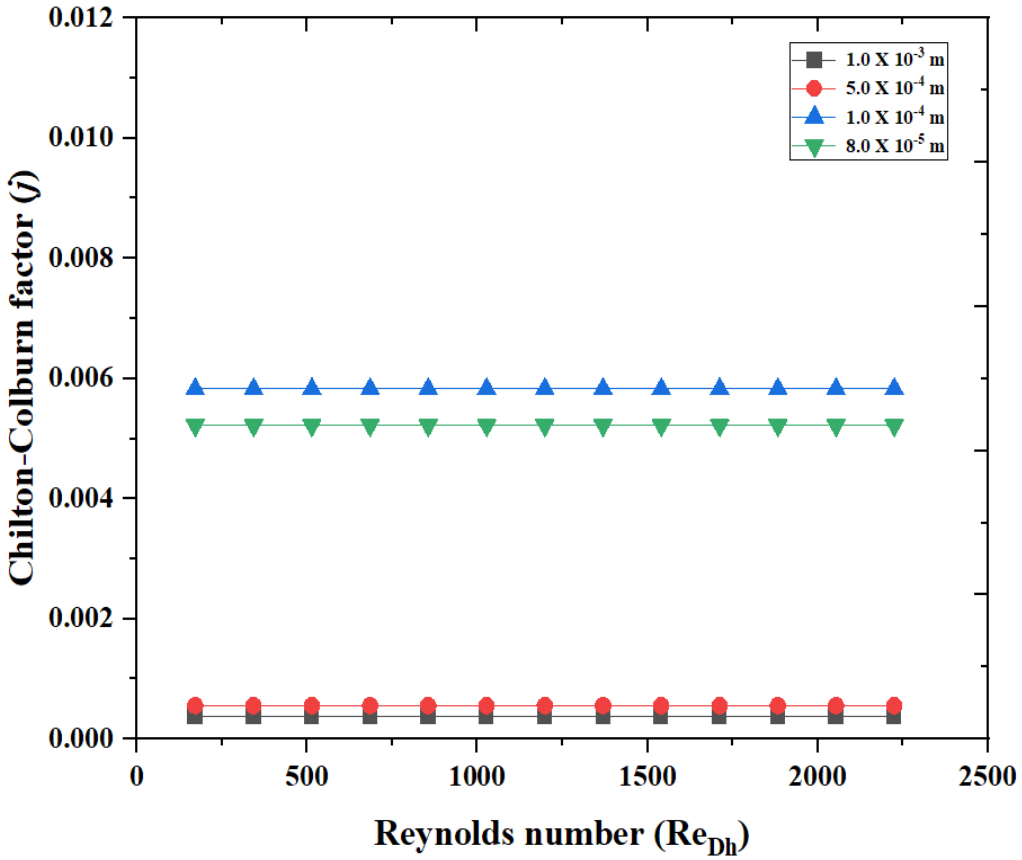

Figure 4.13: Chilton-Colburn Factor (*j*) comparison of different mesh sizes for the 519 fin design.

Figure 4.13 is a comparison of Chilton-Colburn factor *j*. The highest heat transfer rate is with the mesh size of 1.0 x 10^{-4} m, 8.0 x 10^{-5} m followed by 5.0 x 10^{-4} m while the mesh size 1.0 x 10^{-3} m simulation yields the lowest. As shown, the Chilton-Colburn factor *j* of the different mesh size increases slightly with increase in Reynolds number. This inferred that the lower the mesh size, the better heat transfer application.

Again, with the mesh utilized during the numerical stimulations plays a very important role in determining accurate results. The smallest mesh size (8 x 10^{-5} m) provides the most accurate data. Here, we see that the Chilton-Colburn factor *j* or heat transfer rate is relatively constant over the

laminar flow range of Reynolds number tested. We also see that there exists an average percentage difference of 11 – 172.9 % between the three largest mesh sizes (1×10^{-3}, 5×10^{-4}, and 1×10^{-4} m) and the smallest mesh size (8×10^{-5} m) tested. The plot shows the mesh size 1.0×10^{-4} m demonstrate approximately 11% thermal performance than the mesh size 8.0×10^{-5} m unlike other.

4.7 SUMMARY OF RESULT

This thesis research work provided a method to effectively analyze compact heat exchanger fin designs of conceptual design from a CAD drawing to running numerical simulations on the fluid flow to predict friction factor *f* (pressure drop) and Chilton–Colburn factor *j* (heat transfer rate).

1) Verification of using Ansys fluent in the numerical simulations of the laminar flow through seven fin designs.
2) Friction factor *f* results friction factor decreases as Reynolds number Re increases
    - Kays and London (1984) experimental data is greater than Numerical simulations (606, 161, 606Notch, 161Notch).
    - Kays and London (1984) experimental data is approximately equal to 519 and 635 results.
3) Chilton–Colburn factor *j* is equal to heat transfer rate
    - Chilton–Colburn factor *j* relatively constant for laminar flow over the Reynolds number Re range tested; Kays and London (1984); decreases as Reynolds number increases.
    - Kays and London (1984) experimental data is greater than numerical results 606, 161, 606Notch, 161Notch, 635.
    - Kays and London (1984) experimental data is approximately equals 519 results.
4) Mesh sizes
    - Smaller mesh sizes provide best accuracy (1×10^{-3} m, 5×10^{-4} m, 1×10^{-4}, 8×10^{-5} m).
    - 519 fin design 1×10^{-4} m is approximately equal 8×10^{-5} m results for friction factor *f*.

- 635 mesh size of 1 x 10^{-3} m is approximately equal 5 x 10^{-4} m which is not approximately equal to 1 x 10^{-4} m for friction factor *f*.
- 606 and 635 fins not equal to fiction factor *f* and Chilton–Colburn factor *j*, 5 x 10^{-4} m is not approximately equal to 1x 10^{-4} m.

Ansys Fluent define laminar flows as flows characterized by stable velocity fields while Siemens STAR-CCM+ defines it as specifying the properties of the fluids/solid in the model which is an economic way of representing wall functions of boundary layers which indicates the Siemens STAR-CCM+ tends to move it models towards turbulent flow. Therefore, Ansys Fluent provided better CFD predictions for the flows considered in this study.

Also, from the validation of the simulated results view, it is concluded that Ansys Fluent software is more sensitive to laminar flow in compact heat exchanger fins than the STAR-CCM+ software. The STAR-CCM+ software becomes more sensitive in the transitional region. It is also noted, that there is a difference between the numerical simulations in this study compared to the Kays and London (1984) experimental data. This is expected because of experimental uncertainty. The Kays and London (1984) experimental data suggested a transient test technique was employed, and provided uncertainty values of $\pm$5% for both friction factor *f* and Chilton Colburn factor *j*.

The Ansys Fluent numerical simulations detail that the 161Notch fin design provided the best performance of the seven fin designs tested. As summarized in Table 4.6, the 161Notch fin design had the lowest fanning friction factor *f* which implies the lowest pressure drop while the 519 fin design has its Chilton Colburn factor *j* higher than other fins. These are good performance indicators for compact heat exchangers. So the justifications of use will be made over the two performance criteria to select/achieve the desired heat exchanger.

Table 4.6: Summary of ratings of the seven fin designs tested.

FIN DESIGN	Ratings of Friction factor (*f*)
606	5th
606NOTCH	4th
161	2nd
161NOTCH	1st
519	6th
635	7th
Combination of 606 and 635	3rd

Generally, the Chilton Colburn analogy is very helpful for evaluating the heat transfer in internal forced flows. Kumar and Mahulikar (2017); observed that the Chilton Colburn analogy is valid only for that portion of the flow regime; where the Chilton Colburn factor *j* decreases with decreasing fanning friction factor *f*. They further verified this by the inverse dependence of Reynolds number (Re) with fanning friction factor *f*.

From Figures 4.2 to 4.13, it is concluded that the simulated friction for the different results, the friction factors *f*, were all decreasing with increasing Reynolds number. The Chilton Colburn factor *j* did not exhibit the relationship shown experimentally as the Ansys Fluent simulated results showed a very negligible change with Reynolds Number.

However, it is shown that the finer the mesh size, the lower the friction factor *f* which predicts a lower pressure drop across the fin design and a higher heat transfer rate. The finer mesh sizes are more accurately matched the experimental results, indicating that the finer mesh is needed for the best CFD results.

CHAPTER FIVE

CONCLUSIONS AND RECOMMENDATIONS

5.1 CONCLUSIONS

In this study, the CFD method of numerical simulations has been applied to determine the heat transfer and pressure drop characteristics of seven industrial-type compact heat exchangers fin designs. Two CFD software packages were tested with the laminar flow of air through the fin designs. Validated simulation by existing design simulation results to published experimental data. The 161Notch fin design provided the best for lowest friction factor *f*, while the 519 fin design performed best for the highest Chilton Colburn Factor *j*.

As expected, the friction factor *f* was found to decrease with increases in the Reynold number while the Chilton-Colburn factor, *j* remained relatively constant for the laminar flow range of Reynolds number. The mesh size has an improvement in the thermophysical characteristics of the fin design that made up the heat exchangers. The finer the mesh size, the better heat transfer rate and pressure drop predictions.

5.2 RECOMMENDATIONS

This work has shown the feasibility of performing a thermal analysis of compact heat laminar flow in compact heat exchangers. Therefore, there are two possible ways of improving data acquired. First, there should be an improvement in the number of the high performing supercomputing systems utilized because the present Ansys Fluent software depends on memory cores for performance. Alternatively, there could be an upgrade of the Ansys Fluent software that does not depend as much on memory cores.

Secondly, the Kays and London (1984) data are mainly from a transient test technique which is less reliable when considering laminar flow. Future experiments are recommended to update the comparison. A proposed experimental system is next described.

5.3 DESIGN OF PROPOSED EXPERIMENTAL SYSTEM

Experimental analysis is a scientific procedure undertaken to make a discovery, test a hypothesis, or demonstrate a known fact. This method enables the performer to calculate pressure drop (Δp), mass flow rate $\dot{m}$ and wall temperature (T_w) as well as fluid temperatures (T_∞). Figure 5.1 is a schematic of a proposed experimental system that could be used to test the performance of compact heat exchanger fin designs.

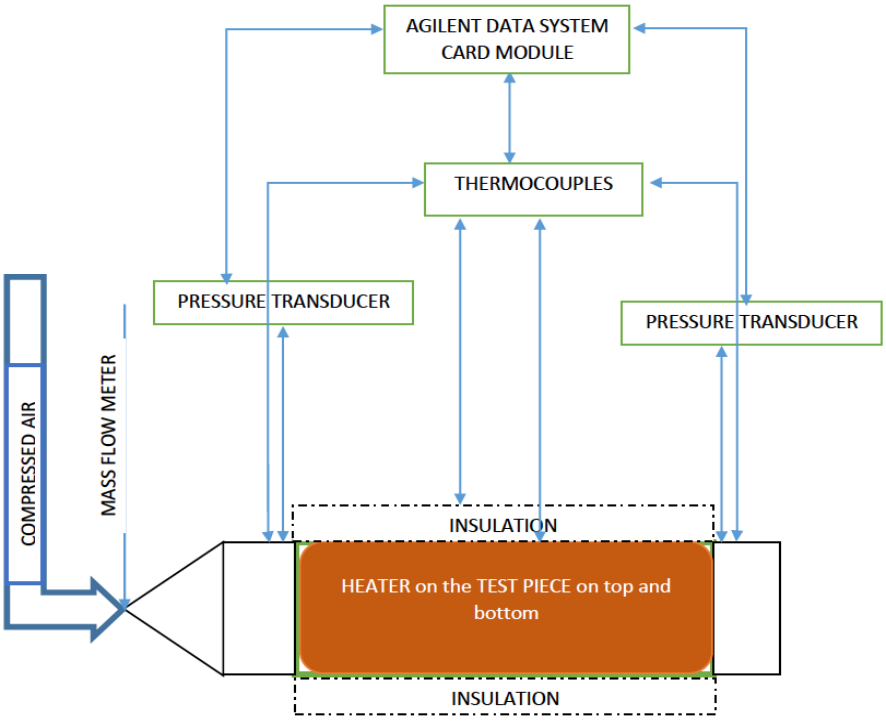

Figure 5.1: Schematic of a proposed experimental setup to test the pressure drop and heat transfer rate of the prototype compact heat exchanger fin designs.

Materials that would be used for the experiment setup include a pivoting steel hose fitting, air-knife, honey comb screen, measurement duct, air control valves, washers, nuts, screws and gaskets/seals. Figure 5.2 shows the exploded view of the experimental apparatus proposed. Samples to be tested will be 12” x 3.5” or more so that fully developed flow can be achieved.

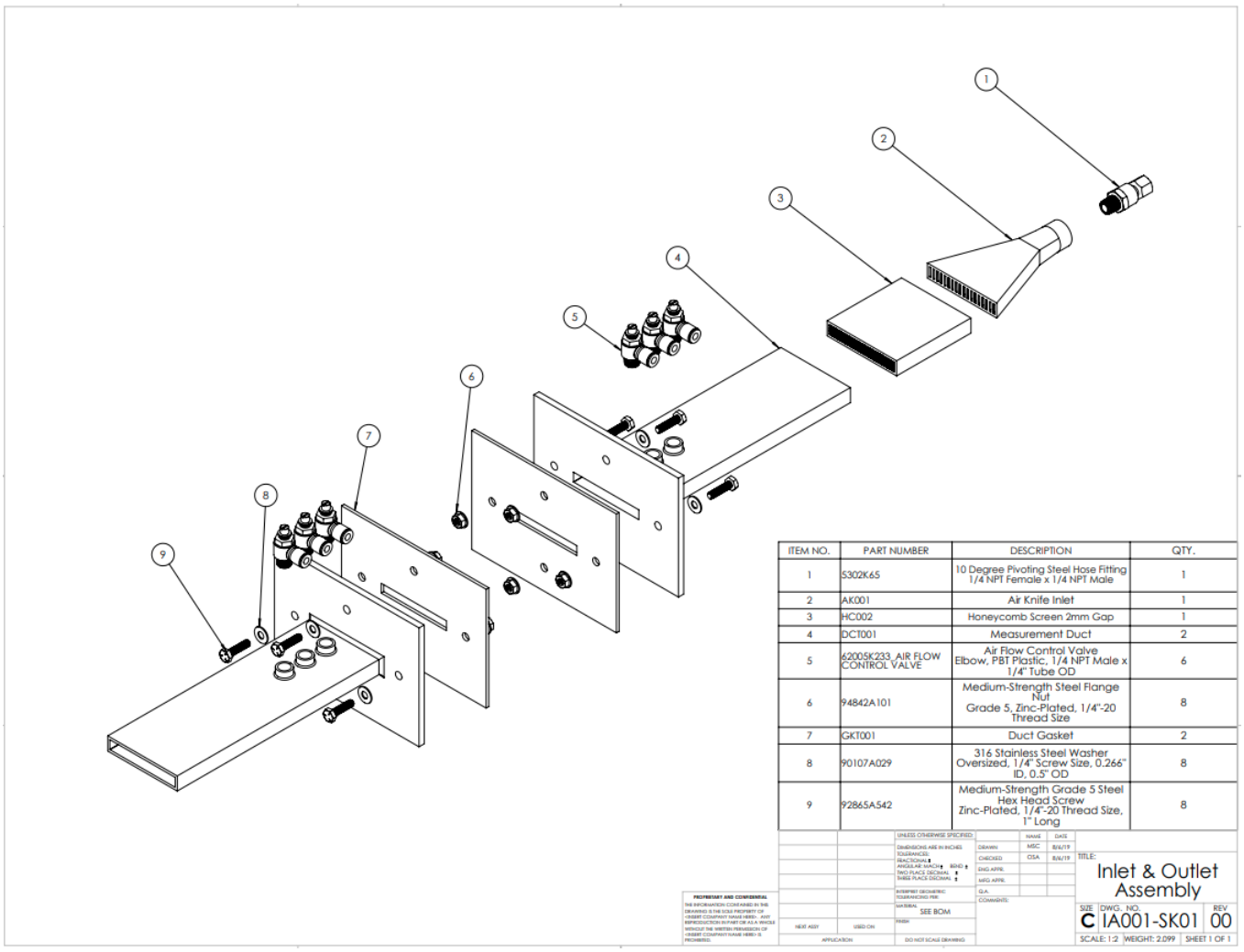

ITEM NO.	PART NUMBER	DESCRIPTION	QTY.
1	5302K65	10 Degree Pivoting Steel Hose Fitting 1/4 NPT Female x 1/4 NPT Male	1
2	AK001	Air Knife Inlet	1
3	HC002	Honeycomb Screen 2mm Gap	1
4	DCT001	Measurement Duct	2
5	62005K233_AIR FLOW CONTROL VALVE	Air Flow Control Valve Elbow, PBT Plastic, 1/4 NPT Male x 1/4" Tube OD	6
6	94842A101	Medium-Strength Steel Flange Nut Grade 5, Zinc-Plated, 1/4"-20 Thread Size	8
7	GKT001	Duct Gasket	2
8	90107A029	316 Stainless Steel Washer Oversized, 1/4" Screw Size, 0.266" ID, 0.5" OD	8
9	92865A542	Medium-Strength Grade 5 Steel Hex Head Screw Zinc-Plated, 1/4"-20 Thread Size, 1" Long	8

Figure 5.2: Exploded view of the proposed experimental apparatus.

UNIFORM DISTRIBUTION OF FLUID

AIR KNIFE

The air knife is a device designed to ensure a perfectly optimized air flow for a range of industrial applications which includes cleaning, drying, blow-off and liquid control. Flow distribution has significant influences on the performance of fluidic devices in many industrial applications. Such

industries include automobiles, electronics, chemistry, metal processing, packaging, paper printing, micro-channel reactors, plate-type heat exchangers, and fuel cells, etc.

At present, air knives are an important piece of equipment used for the deep and fine processing of products. Featured with low costs, uniform airflow, simple structure, easy installation, and effective reduction of energy loss, air knives are favoured by various researcher (Xiang, 2013).

Better heat transfer and temperature control, low pressure losses (which means less pumping power), and a minimization of energy dissipation can be provided through uniform flow distribution, especially for the numbering up of devices for industrial-scale applications with thousands of parallel channels.

The air knife shoots a wide flat band of air (or coolant) and much quieter than a standard nozzle. A schematic diagram of the air knife shape bifurcation distributor is shown in Figure 5.3. The following parameters are used to identify the geometry of the flow distributor:

A = inlet orifice,

B = throat of the knife,

b = value of bifurcation angle,

w = half-width of the knife,

c and *b* = the channel width.

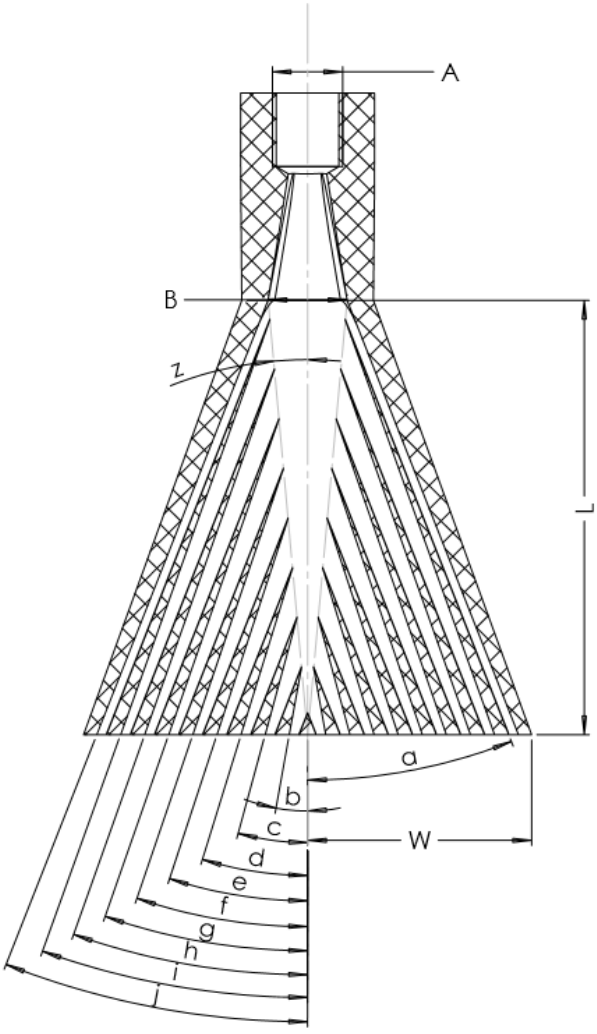

Figure 5.3: Schematic of proposed air-knife structure.

HONEYCOMB

Honeycomb is known as a flow straightener, implying is a device used to straighten the air flow in a wind tunnel. It is a passage of ducts, laid along the axis of main air stream to minimize the lateral velocity components caused by swirling motion in the air flow during entry. The cross-section shapes of these "honeycombs" may be of square, circular and regular hexagonal cells as shown in Figure 5.4**.**

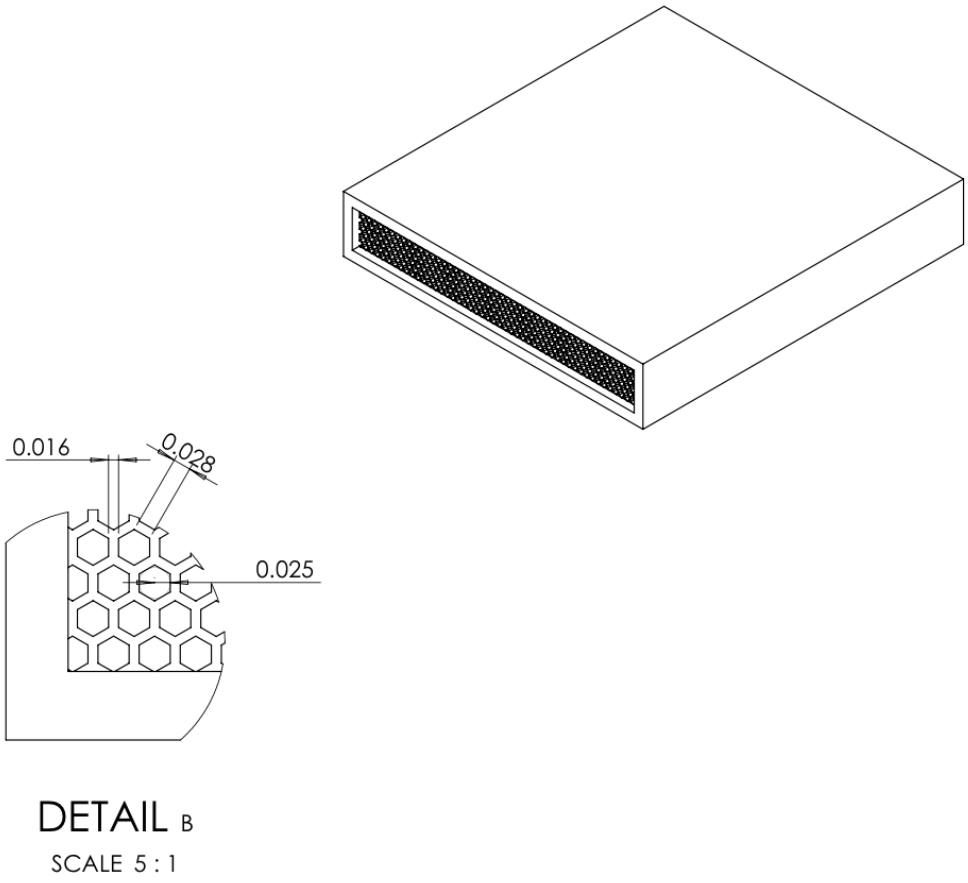

Figure 5.4: Schematic of the proposed Honeycomb flow straightener.

The effectiveness of the honeycomb in reducing the swirl and turbulence level is studied by simulating the flow field using standard k-ε turbulence model in commercial computational fluid dynamics (CFD). CFD is the most precise and economical approach to estimate the effectiveness of a honeycomb.

A honeycomb has two effects on a flow stream: (1) it reduces the level of the existing turbulence and (2) it creates additional turbulence of its own. Analyses have been developed for prediction of these effects, including estimates of the change in turbulence levels between a wind tunnel plenum and test section due to the intervening decay length and the effect of the tunnel contraction

(Lumley, 1964, McMahon,1967). Robbins (1978) provided experimental verification for the analysis that showed that the predictions for the turbulence reduction and production by a honeycomb assuming that the flow in the honeycomb cells is fully developed turbulent. At Reynolds numbers near the turbulence transition in the honeycomb cells, incidentally, higher levels of turbulence and mean velocity nonuniformity may result in the test section as a consequence of transition occurring nonuniformly across the honeycomb (Robbins, 1978).

The length-to-diameter ratio of the honeycombs was chosen as 6 or 8 on the basis of the laminar cell flow results but the cell Reynolds of these experiments are in the transition range or higher (Loehrke, 1972).

REFERENCES

Amano, R. S. (1985). A Numerical Study of Laminar and Turbulent Heat Transfer in a Periodically Corrugated Wall Channel. *Jouranl Heat Transfer. 107(3),* 564 - 569.

ANSYS. (2011). Fluent. Retrieved 03 28, 2018, from https://www.ansys.com: https://www.ansys.com/-/media/ansys/corporate/resourcelibrary/brochure/ansys-Fluent-brochure-140.pdf

ANSYS. (2018). Lecture 1.2: Overview of the CFD Process and Workflow: ANSYS Fluent Getting Started. Canonsburg: ANSYS LEARNING HUB.

Ansys, I. (2018). ANSYS Fluent Getting Started Guide. Canonsburg, PA: ANSYS, Inc. and ANSYS Europe, Ltd. .

Bejan, A. (2000). Shape and Structure, From Engineering to Nature. Cambridge, UK: Cambridge University Press.

Bergles, A. M. (1995). Heat transfer and pressure drop correlations for the rectangular offset strip fin compact heat exchanger. *Experimental Thermal and Fluid Science, Vol. 25, Issues. 2,* 171 - 180.

Bergman, T. L. (2017). Fundamentals of Heat and Mass Transfer. Hoboken, NJ: John Wiley & Sons, Inc.

Bhowmik, H. L. (2009). Analysis of heat transfer and pressure drop characteristics in an offset strip fin heat exchanger. *International Community. Heat Mass Transfer, 36(3),* 259 - 263.

Briggs, D. L. (1961). The heat transfer and flow friction characteristics of five offset rectangular duct and six plain triangular plate-fin heat transfer surfaces. *International Development Heat Transfer,* Volume. 125, 122 – 134.

Chakraborty, S. R. (2011). Performance optimization of laminar fully developed flow through square ducts with rounded corners. *International Journal Therm Sci 50,* 2522 - 2535.

Chen, B. H. (1988). Performance-Evaluation Criteria for Enhanced Heat-Transfer Surfaces. *International Community Heat Mass 15*, 59 - 72.

Cowell, T. A. (1990). A General Method for the Comparison of Compact Heat Transfer Surfaces. *Journal of Heat Transfer | Volume 112 | Issue 2,* 288 - 294 .

Dimitrios, S. (2013, 09 21 - 27). *Express Introductory Training in ANSYS Fluent Lecture 2 Boundary Conditions & Solver Settings.* Retrieved from https://events.prace-ri.eu: https://events.prace-ri.eu/event/156/contributions/6/attachments/65/89/Fluent-Intro_14.5_L02_BoundaryConditionsSolverSettings.pdf

Dubrovsky, E. V. (1988). Enhancement of convective heat transfer in rectangular ducts of interrupted surfaces. *International Journal of Heat and Mass Transfer,* Volume 31, Issue 4, 807 - 818.

Gongnan, X. F. (2014). Constructal design and thermal analysis of microchannel heat sinks with multistage bifurcations in single-phase liquid flow. *Applied Thermal Engineering*, Volume 62, Issue 2, 791 - 802.

Guo, K. Z. (2014). Optimisation of fin selection and thermal design of plate-fin heat exchangers. *Chemical Engineering. Transactions* Volume 39, 325 – 330.

Hong, L. P.-R. (2012). Experimental study of the flow distribution uniformity in flow distributors having novel flow channel bifurcation structures. *Experimental Thermal and Fluid science* Volume 37, 142 - 153.

Hou, K. (1988). Thermal Performance of Offset Strip Fins under Unsymmetrical Heating Condition for Various Fluids. Long Beach: California State University, Master Thesis, .

Huizhu, Y. J. (2018). Effect of fin types and Prandtl number on performance of plate-fin heat. *Applied Thermal Engineering* Volume 144, 726 - 735.

Jian, Q. C. (2020, April 05). Simulation analysis on inner flow field and optimization design of air knife. Retrieved from JVE Journals: https://www.jvejournals.com/article/18242

Jiao, A. R. (2003). Experimental investigation of header configuration on flow maldistribution in plate-fin heat exchanger. *Applied Thermal Engineering,* 1235 - 1246.

Jiawen, Y. H. (2017). A numerical study of heat transfer and pressure drop of hydrocarbon mixture refrigerant during boiling in vertical rectangular minichannel. *Applied Thermal Engineering,* Volume 122, 1343 - 1352.

Joshi, H. R. (1987). Heat transfer and friction in the offset stripfin heat exchangers. *International Journal Heat Mass Transfer 30*, 69 - 84.

Jun, C. M. (2018). Numerical analysis on the effect of bifurcation angle and inlet velocity onthe distribution uniformity performance of consecutive bifurcating fluidflow distributors. *International Communications in Heat and Mass Transfer Volume 93*, 60 - 65.

Junqi, D. J. (2007). Air-side thermal hydraulic performance of offset strip fin aluminum heat exchangers. *Applied Thermal Engineering, Volume 27,* 306 - 313.

Kays, W. M. (2012). The Basic Heat Transfer and Flow Friction Characteristics of Six Compact High-Performance Heat Transfer Surfaces. *Journal of Engineering for Power,* Volume 82 | Issue 1 , 27 - 34.

Kays, W. M. (1989). Compact Heat Exchangers. Malabar, Florida: Krieger publishing company

Khoshvaght-Aliabadi, M. H. (2014). Role of channel shape on performance of plate-fin heat exchangers: Experimental assessment. *International Journal of Thermal Sciences 79*, 183-193.

Kim, M.-S. J.-J.-S. (2011). Correlations and optimization of a heat exchanger with offset-strip fins. *International Journal of Heat and Mass Transfer*, 2073 - 2079.

Kwon, S. B. (2009). Numerical analysis for the coating thickness prediction in continuous hot-dip galvanizing. *Journal of Mechanical Science and Technology,* Volume. 23, Issue 12, 3471 - 3478.

Lacanette, D. V. (2005). Numerical simulation of gas-jet wiping in steel strip galvanizing process. *ISIJ International* Volume 45 Issue 2, 214 - 220.

Lalot, S. F. (2003). Experimental investigation of header configurationon flow maldistribution in plate-fin heat exchanger. *Applied Thermal Engineering*, 1235 - 1246.

Latife, B. E. (2017). Comprehensive Study of Compact Heat Exchangers with Offset Strip Fin. In *Heat Exchangers– Advanced Features and Applications* (pp. 30 - 59). London: IntechOpen Limited.

Lee, H. (2010). *Thermal Design Heat Sinks, Thermoelectrics, Heat Pipes, Compact Heat Exchangers, and Solar Cells.* New Jersey: John Wiley & Sons, Inc.

Lee, H. W. (2016). A study on high speed coupling design for wind turbine using a finite element analysis. *Journal of Mechanical Science and Technology*, Volume 30, Issue 8, 3713 - 3718.

Lijun, W. W. (2013). Numerical and experimental investigation of mixing characteristics in the constructal tree-shaped microchannel. *International Journal of Heat and Mass Transfer*, Volume 67, 1014 - 1023.

Liu, P. ,. (2016). A theoretical model to predict frosting limits in cross-flow air-to-air flat plate heat/energy exchangers. *Energy and Buildings,* Volume 110, Issue 1, 404 - 414.

Loehrke, R. I. (1972). Experiments on Management of Free-Stream Turbulence. NATO: AGARD Report No. 598.

London, A k. (1998). Compact Heat Exchangers. Florida: KRIEGER Publishing Company.

Lumley, J. L. (1964). Passage of a Turbulent Stream Through Honeycomb of Large Length-to-Diameter Ratio. *Journal of Basic Engineering, Transaction of ASME,* Series D, Volume. 86, 218 - 220.

Luo, L. Z. (2008). Experimental study of constructal distributor for flow equidistribution in a mini crossflow heat exchanger (MCHE). *Chemical Engineering and Processing: Process Intensification*, Volume 67, 229 - 236.

Manglik, R. M. (1995). Heat transfer and pressure drop correlations for the rectangular offset strip fin compact heat exchanger. *Experimental Thermal and Fluid Science,* Volume. 10, Issues. 2, 171 - 180.

McMahon, J. L. (1967). Reducing water Tunnel Turbulence by Means of a Honeycomb. *Journal of Basic Engineering, Transaction of ASME,* Series D, Volume. 89, 764 - 770.

Mori, Y. N. (1980). Recent Advances in Compact Heat Exchangers in Japan. *The American Society of Mechanical Engineers*, 5-16.

Mueller, A. C. (1988). Review of various types of flow maldistribution in Heat Exchangers. *Heat Transfer Engineering,* Volume 9, 36 - 50.

Nakonieczny, K. (2006). Numerical modeling of cross-flow plate-fin air-to-air heat exchanger under unsteady flow conditions. *Numerical Heat Transfer Part A, 49,* 1 - 24.

Nouidui, T. P. (2012). Modelica Buildings library. *Journal of Building Performance Simulation,* 253 - 270.

Patankar, S. V. (1977). Fully Developed Flow and Heat Transfer in Ducts Having Streamwise-Periodic Variations of Cross-Sectional Area. *Journal Heat Transfer. 99(2),* 180 - 186.

Peng, H. X. (2008). Optimal design approach for the plate-fin heat exchangers using neural networks cooperated with genetic algorithms. *Applied Thermal Engineering,* Volume 28, Issues 5 - 6, 642-650.

Picon-Nunez, M. P.-F. (2002). Thermal design of multi-stream heat exchangers. *Applied Thermal Engineering,* Volume 22, Issues 14, 1643 - 1660.

Pistoresi, C. F. (2015). Numerical study on the improvement of flow distribution uniformity among parallel mini-channels. *Chemical Engineering and Processing: Process Intensification*, Volume 95, 63 - 71.

Pua, L. ,. (2002). Integrated heat exchanger network and equipment design using compact heat exchanger. *Heat Transfer Engineering,* Volume 23, Issues 6 , 18 – 35.

Qi, H. Y. (2014). Improvement of the air knife close-loop control system. *Steel Rolling,* Volume. 31, Issue 2, 65 - 66.

Raju, K. S. (2011). Fluid Mechanics, Heat Transfer, and Mass Transfer: Chemical Engineering Practice, . New Jersey: John Wiley & Sons, Inc.

Rammer, T. N. (2009). Dynamic model of counter flow air to air heat exchanger for comfort ventilation with condensation and frost formation. *Applied Thermal Engineering*, Volume 29, Issues 2 - 3, 462 - 468.

Robbins, B. E. (1978). Water Tunnel Turbulence Measurements Behind a Honeycomb. *Journal Hydronautics,* Volume 12,, 122 - 128.

Rose, J. N. (2008). Quasi-steady-state model of a counter-flow air-to-air heat-exchanger with phase change. *Applied Energy,* Volume 85, Issue 5, 312 - 325.

Safikhani, H. A.-B. (2010). Numerical simulation of flow field in three types of standard cyclone separators. *Advanced Powder Technology,* Volume 21, Issue 4, 435 - 442.

Seongho, P. I.-J. (2016). Design of microchannel Fischer–Tropsch reactor using cell-couplingmethod: Effect of flow configurations and distribution. *Chemical Engineering Science*, Volume 143, 63 - 75.

Shah, R. (1982). Compact heat exchanger selection method, advances in compactheat exchanger technology and design theory. *6th International Heat Transfer Conference* (pp. 193 – 199.). Toronto, Hemisphere Publisher.

Shah, R. K. (1967). Offset Rectangular Plate-Fin Surfaces—Heat Transfer and Flow Friction Characteristics. *Journal of Engineering for Power,* Volume 90 | Issue 3, 218 - 228.

Shah, R. K. (2007). Fundamentals of Heat Exchanger Design. Hoboken, NJ, USA: John Wiley & Sons, Inc.

Shao, J. C. (2007). Numerical analysis of the flow around a circular cylinder using RANS and LES. *International Journal of Computational Fluid Dynamics*, 301 - 307.

Shehab, S. N. (2017). Experimental Study of Free-Convection from Rectangular Fins Array on a Heated Horizontal Plate with. Baghdad: Mechanical Engineering Department, Engineering College.

Shujan, M. A. (2016). Cfd basic & Use of ANSYS FLUENT in Engineering Application: A brief Introduction. Retrieved 03 28, 2018, from https://www.slideshare.net: https://www.slideshare.net/muhammadshujan/cfd-Ansys-Fluent

Sun, Y. H. (2013). Gas flow dynamic study on air knife of vertical glass cleaner. *Journal of North China University of Technology*, Volume 25, Issue 3, 50 - 55.

Suzuki, K. H. (1985). Numerical and experimental studies on a two-dimensional model of an offset-strip-fin type compact heat exchanger used at low Reynolds number. *International Journal of Heat and Mass Transfer* Volume. 28 Issue 4, 823 - 836.

Szücs, L. H. (1962, 06 11). Heat Transfer In Compact Plate-Fin Heat Exchangers. *Periodica Polytechnica Mechanical Engineering*, pp. 21 - 36.

Tagliafico, L. T. (1996). Thermodynamic method for the comparison of plate-fin heat exchanger performance. *Journal Heat Transfer 118*, 805 - 911.

Tan-atichat, J. N. (1982). Interaction of Free-Stream Turbulence with Screens and Grids: A Balance Between Turbulence Scales. *Journal Fluid Mechanics*, Volume 114, 501 - 528.

Taylor, M. (1990). Plate-Fin Heat Exchangers, Guide to Their Specification and Use. Oxon, U.K: HTFS (Harwell Laboratory).

Wang, L. X. (2016). Optimal design for split-and-recombine-type flow distributors of microreactors based on blockage detection. *Chinese Journal of Chemical Engineering*, Volume 27, 897 - 903.

Wei, W. D. (2017). Experimental study and optimization of pin fin shapes in flow boiling of micro pin fin heat sinks. *Applied Thermal Engineering, Volume 114*, 436 - 449.

Wen, J. H. (2016). Optimization investigation on configuration parameters of serrated fin in plate-fin heat exchanger using genetic algorithm. *International Journal of Thermal Sciences*, Volume 101, 116 - 125.

Wetter, M. (1999). *Air-to-Air Plate Heat Exchanger.* Berkeley: Simulation Research Group, Building technologies Department Environmental Energy.

White, F. M. (2017). *Fluid Mechanics.* Florida, USA: CRC.

Williamson, C. (1996). Vortex dynamics in the cylinder wakes. *Annual Review Fluid Mechanics,* Volume 28, 477–539.

Xiang, W. J. (2013). Velocity calibration and investigation of flow field at air knife exit. *Journal of Atmospheric and Environmental Optics*, Volume 8, 321 - 326.

Xiaofeng, G. L. (2014). Multi-channel heat exchanger- reactor using arborescent distributors: A characterization study of fluid distribution, heat exchange performance and exothermic reaction. *Energy*, Volume 69, 728 - 741.

Xilong, Z. Y. (2015). Numerical analysis of thermal-hydraulic characteristics on serrated fins with different attack angles and wavelength to fin length ratio. *Applied Thermal Engineering*, Volume 91, 126 - 137.

Yidan, S. M. (2015). Constructal wavy-fin channels of a compact heat exchanger with heattransfer rate maximization and pressure losses minimization. *Applied Thermal Engineering*, Volume 75, 24 - 32.

Yohannes, G. J. (2011). Asymmetrical flow field-flow fractionation technique for separation and characterization of biopolymers and bioparticles. *Journal of Chromatography A*, Volume 1218, Issue 27, 4104 - 4116.

Yousefi, M. R. (2013). Optimization of plate-fin heat exchangers by an improved harmony search algorithm. *Applied Thermal Engineering 50*, 877 - 885.

Yousefia, M. ,. (2013). Optimization of plate-fin heat exchangers by an improved harmony search algorithm. *Applied Thermal Engineering*, Volume. 50, Issue 1, 877 - 885.

Yousefia, M. E. (2012). Optimal design of plate-fin heat exchangers by a hybrid evolutionary algorithm. *International Communications in Heat and Mass Transfer*, Volume. 39, Issue. 2, 258 - 263.

Yujie, Y. Y. (2014). General prediction of the thermal hydraulic performance for plate-fin heat exchanger with offset strip fins. *International Journal of Heat and Mass Transfer*, 860 - 870.

Zdravkovich, M. M. (1997). *low Around Circular Cylinders.* Oxford,England: Oxford University Press Inc.

Zhiwei, F. X. (2008). Experimental investigation of the flow distribution of a 2-dimensional constructal distributor. *Experimental Thermal and Fluid Science*, Volume 33, 77 - 83.

Zhong, H. F. (2002). The development of hot-dip galvanized strip technology abroad. *Corrosion and Production,* Volume. 23, Issue 11,, 74 - 478.

Zimparov, V. (2001). Enhancement of heat transfer by a combination of three-start spirally corrugated tubes with a twisted tape. *International Journaal Heat Mass Transcation 44*, 169 - 180.

APPENDIX

This section provides the table of value used to plot all the graphs used in this thesis. It contains both the Ansys Fluent data and STAR-CCM+ data.

Table A.1: Comparison of the 606, 161 fin designs against the data of Kays and London (1984) 606 Friction factor (*f*).

Friction factor *(f)*					
Reynolds number	**606 Fluent**	**606 STAR-CCM+**	**161 Fluent**	**161 STAR-CCM+**	**Kays & London (1984) 606**
183.5	0.0699	0.8621	0.0464	0.8818	0.2038
367.0	0.0350	0.4975	0.0221	0.4577	0.1616
550.5	0.0233	0.3634	0.0143	0.3121	0.1239
734.0	0.0175	0.2921	0.0106	0.2384	0.107
917.5	0.0140	0.2479	0.0085	0.1971	0.0965
1101.0	0.0117	0.2175	0.0067	0.1686	0.0898
1284.6	0.010	0.1951	0.0059	0.1484	0.0855
1468.0	0.0087	0.1781	0.0053	0.1339	0.0823
1651.6	0.0078	0.1648	0.0047	0.1231	0.0801
1835.1	0.0070	0.1539	0.0042	0.1144	0.0782
2018.6	0.0064	0.1448	0.0038	0.1066	0.0764
2202.1	0.0058	0.1372	0.0034	0.0988	0.0752
2385.6	0.0054	0.1297	0.0030	0.0910	0.0740

Table A.2: Comparison of the 606, 161 fin designs against the data of Kays and London (1984) 606 Chilton-Colburn Factor (*j*).

Chilton-Colburn Factor (*j*)					
Reynolds number	**606 Fluent**	**606 STAR-CCM+**	**161 Fluent**	**161 STAR-CCM+**	**Kays & London (1984) 606**
183.5	0.0039	0.7389	0.0038	3.4575	0.0277
367.0	0.0039	0.1321	0.0038	0.5487	0.0252
550.5	0.0039	0.0481	0.0038	0.1834	0.0228
734.0	0.0039	0.0238	0.0038	0.0852	0.0210
917.5	0.0039	0.0140	0.0038	0.0508	0.0197
1101.0	0.0039	0.0092	0.0038	0.0330	0.0186
1284.6	0.0039	0.0064	0.0038	0.0228	0.0177
1468.0	0.0039	0.0048	0.0038	0.0166	0.0170
1651.6	0.0039	0.0037	0.0038	0.0128	0.0164
1835.1	0.0039	0.0029	0.0038	0.0101	0.0159
2018.6	0.0039	0.0024	0.0038	0.0078	0.0155
2202.1	0.0039	0.0020	0.0038	0.0055	0.0151
2385.6	0.0039	0.0016	0.0038	0.0033	0.0147

Table A.3: Comparison of the 606Notch, 161Notch fin designs against the Kays and London (1984) data 606 Friction factor (*f*).

Friction Factor (*f*)					
Reynolds number	**606 Notch Fluent**	**606 Notch STAR-CCM+**	**161 Notch Fluent**	**161 Notch STAR-CCM+**	**Kays & London (1984) 606**
183.5	0.0635	0.8342	0.0452	0.9052	0.2038
367.0	0.0317	0.4669	0.0235	0.5006	0.1616
550.5	0.0212	0.3299	0.0209	0.3567	0.1239
734.0	0.0159	0.2587	0.0110	0.2814	0.1070
917.5	0.0127	0.2156	0.0088	0.2339	0.0965
1101.0	0.0106	0.1875	0.0073	0.2010	0.0898
1284.6	0.0091	0.1680	0.0063	0.1768	0.0855
1468.0	0.0079	0.1539	0.0055	0.1583	0.0823
1651.6	0.0071	0.1432	0.0049	0.1437	0.0801
1835.1	0.0064	0.1349	0.0044	0.1318	0.0782
2018.6	0.0058	0.1282	0.0040	0.1219	0.0764
2202.1	0.0053	0.1228	0.0037	0.1136	0.0752
2385.6	0.0049	0.1182	0.0033	0.1056	0.0740

Table A.4: Comparison of the 606Notch, 161Notch fin designs against the Kays and London (1984) 606 data Chilton-Colburn factor (*j*).

Chilton-Colburn Factor (*j*)					
Reynolds number	**606 Notch Fluent**	**606 Notch STAR-CCM+**	**161 Notch Fluent**	**161 Notch STAR-CCM+**	**Kays & London (1984) 606**
183.5	0.0040	2.1837	0.0038	0.5590	0.0277
367.0	0.0040	0.5497	0.0038	0.1003	0.0252
550.5	0.0040	0.2502	0.0038	0.0370	0.0228
734.0	0.0040	0.1452	0.0038	0.0184	0.0210
917.5	0.0040	0.0962	0.0038	0.0110	0.0197
1101.0	0.0040	0.0691	0.0038	0.0070	0.0186
1284.6	0.0040	0.0525	0.0038	0.0049	0.0177
1468.0	0.0040	0.0416	0.0038	0.0036	0.0170
1651.6	0.0040	0.0339	0.0038	0.0027	0.0164
1835.1	0.0040	0.0283	0.0038	0.0021	0.0159
2018.6	0.0040	0.0241	0.0038	0.0017	0.0155
2202.1	0.0040	0.0209	0.0038	0.0014	0.0151
2385.6	0.0040	0.0183	0.0038	0.0011	0.0147

Table A.5: Comparison of the 519-fin design against the Kays and London (1984) data 519 Friction Factor (*f*).

Friction factor (*f*)			
Reynolds number	**519 Fluent**	**519 STAR-CCM+**	**Kays & London (1984) 519**
171.2	0.1183	0.5240	0.0571
342.3	0.0592	0.2085	0.0486
513.4	0.0394	0.1989	0.0400
684.6	0.0296	0.1565	0.0321
855.7	0.0237	0.1184	0.0329
1026.9	0.0197	0.1047	0.0244
1198.0	0.0169	0.0994	0.0232
1369.2	0.0148	0.0858	0.0218
1540.3	0.0132	0.0790	0.0204
1711.5	0.0118	0.0734	0.0189
1882.6	0.0108	0.0686	0.0188
2053.8	0.0099	0.0645	0.0187
2224.9	0.0091	0.0604	0.0185

Table A.6: Comparison of the 519-fin design against the Kays and London (1984) 519 data Chilton-Colburn Factor (*j*).

Chilton-Colburn Factor (*j*)			
Reynolds number	**519 Fluent**	**519 STAR-CCM+**	**Kays & London (1984) 519**
171.2	0.0058	0.0171	0.0178
342.3	0.0058	0.0017	0.0154
513.4	0.0058	9.1784E-4	0.0130
684.6	0.0058	8.1801E-4	0.0111
855.7	0.0058	5.0756E-4	0.0098
1026.9	0.0058	3.4492E-4	0.0088
1198.0	0.0058	2.1551E-4	0.0082
1369.2	0.0058	1.8851E-4	0.0076
1540.3	0.0058	1.3592E-4	0.0073
1711.5	0.0058	1.1834E-4	0.007
1882.6	0.0058	9.3322E-5	0.007
2053.8	0.0058	7.9110E-5	0.007
2224.9	0.0058	6.5722E-5	0.007

Table A.7: Comparison of the 635-fin design against the Kays and London (1984) 635 data Friction Factor (*f*).

Friction factor (*f*)			
Reynolds number	**635 Fluent**	**635 STAR-CCM+**	**Kays & London (1984) 635**
145.1	0.3845	0.1700	0.0954
290.3	0.1922	0.1111	0.0885
435.4	0.1282	0.0868	0.0816
580.5	0.0961	0.0724	0.0747
725.7	0.0769	0.0628	0.0678
870.8	0.0641	0.0557	0.0620
1015.9	0.0549	0.0503	0.0574
1161.1	0.0481	0.046	0.0539
1306.2	0.0427	0.0425	0.0505
1451.3	0.0384	0.0396	0.0485
1596.5	0.0350	0.0372	0.0465
1741.6	0.0320	0.0351	0.0445
1886.7	0.0296	0.0331	0.0425

Table A.8: Comparison of the 635-fin design against the Kays & London (1984) 635 data Chilton-Colburn Factor (*j*).

Chilton-Colburn Factor (*j*)			
Reynolds number	**635 Fluent**	**635 STAR-CCM+**	**Kays & London (1984) 635**
145.1	0.0029	1.4960	0.0194
290.3	0.0029	0.3569	0.0183
435.4	0.0029	0.0653	0.0171
580.5	0.0029	0.0940	0.0160
725.7	0.0029	0.0607	0.0148
870.8	0.0029	0.0422	0.0137
1015.9	0.0029	0.0312	0.0128
1161.1	0.0029	0.0248	0.0122
1306.2	0.0029	0.0196	0.0115
1451.3	0.0029	0.0156	0.0111
1596.5	0.0029	0.0127	0.0107
1741.6	0.0029	0.0112	0.0103
1886.7	0.0029	0.0102	0.0100

Table A.9: Comparison of the Combination (606 & 635) fin design Friction Factor (*f*).

Friction factor (*f*)		
Reynolds number	**Combination (606 & 635) Fluent**	**Combination (606 & 635) STAR-CCM+**
164.3	0.0674	0.7209
328.6	0.0337	0.4096
492.9	0.0225	0.2997
657.2	0.0167	0.2425
821.5	0.0135	0.2074
985.8	0.0112	0.1834
1150.1	0.0096	0.1749
1314.4	0.0084	0.1524
1478.7	0.0075	0.1418
1643.0	0.0067	0.1332
1807.3	0.0061	0.1262
1971.6	0.0056	0.1202
2135.9	0.0052	0.1145

Table A.10: Comparison of the Combination (606 & 635) fin design Chilton-Colburn Factor (*j*).

Chilton-Colburn Factor (*j*)		
Reynolds number	**Combination (606 & 635) Fluent**	**Combination (606 & 635) STAR-CCM+**
164.3	0.0039	0.0074
328.6	0.0039	0.0014
492.9	0.0039	5.1892E-4
657.2	0.0039	2.5814E-4
821.5	0.0039	1.5134E-4
985.8	0.0039	9.8322E-5
1150.1	0.0039	6.8501E-5
1314.4	0.0039	5.0192E-5
1478.7	0.0039	3.8199E-5
1643.0	0.0039	2.9944E-5
1807.3	0.0039	2.4038E-5
1971.6	0.0039	1.9677E-5
2135.9	0.0039	1.5564E-5

Table A.11: Comparison of the 606, 635, Combination (606 & 635) fin design against the Kays and London 606 (1984) data Friction Factor (*f*) respectively.

Friction Factor (*f*)								
Reynolds number	**606 Fluent**	**606 STAR-CCM+**	**Kays and London (1984) 606**	**635 Fluent**	**635 STAR-CCM+**	**Kays and London (1984) 635**	**Combination (606 & 635) Fluent**	**Combination (606 & 635) STAR-CCM+**
183.5	0.0699	0.8621	0.2038	0.3336	0.1544	0.0936	0.0635	0.6845
367.0	0.0350	0.4975	0.1616	0.1583	0.0982	0.0849	0.0311	0.3839
550.5	0.0233	0.3634	0.1239	0.1027	0.0754	0.0762	0.0205	0.2797
734.0	0.0175	0.2921	0.1070	0.0762	0.0623	0.0675	0.0153	0.2261
917.5	0.0140	0.2479	0.0965	0.0611	0.0540	0.0605	0.0122	0.1933
1101.0	0.0117	0.2175	0.0898	0.0509	0.0478	0.0554	0.0101	0.1774
1284.6	0.0100	0.1951	0.0855	0.0435	0.0430	0.0510	0.0087	0.1565
1468.0	0.0087	0.1781	0.0823	0.0380	0.0394	0.0482	0.0076	0.1425
1651.6	0.0078	0.1648	0.0801	0.0338	0.0364	0.0457	0.0067	0.1329
1835.1	0.0070	0.1539	0.0782	0.0305	0.0338	0.0432	0.0060	0.1252
2018.6	0.0064	0.1448	0.0764	0.0273	0.0312	0.0407	0.0055	0.1186
2202.1	0.0058	0.1372	0.0752	0.0242	0.0287	0.0381	0.0050	0.1122
2385.6	0.0054	0.1297	0.0740	0.0211	0.0261	0.0356	0.0045	0.1057

Table A.12: Comparison of the 606, 635, Combination (606 & 635) fin design against the Kays and London (1984) data Chilton-Colburn Factor (*j*) respectively.

Chilton-Colburn Factor (*j*)								
Reynolds number	**606 Fluent**	**606 STAR-CCM+**	**Kays & London 606 (1984)**	**635 Fluent**	**635 STAR-CCM+**	**Kays and London 635 (1984)**	**Combination (606 & 635) Fluent**	**Combination (606 & 635) STAR-CCM+**
183.5	0.0039	0.7389	0.0277	0.0029	1.1948	0.0191	0.0039	0.0067
367.0	0.0039	0.1321	0.0252	0.0029	0.2027	0.0177	0.0039	0.0012
550.5	0.0039	0.0481	0.0228	0.0029	0.0881	0.0162	0.0039	4.2746E-4
734.0	0.0039	0.0238	0.0210	0.0029	0.0596	0.0147	0.0039	2.0820E-4
917.5	0.0039	0.0140	0.0197	0.0029	0.0387	0.0134	0.0039	1.2035E-4
1101.0	0.0039	0.0092	0.0186	0.0029	0.0275	0.0124	0.0039	7.7405E-5
1284.6	0.0039	0.0064	0.0177	0.0029	0.0204	0.0116	0.0039	5.3519E-5
1468.0	0.0039	0.0048	0.0169	0.0029	0.0152	0.0111	0.0039	3.8976E-5
1651.6	0.0039	0.0037	0.0164	0.0029	0.0121	0.0106	0.0039	2.9636E-5
1835.1	0.0039	0.0029	0.0159	0.0029	0.0106	0.0101	0.0039	2.3301E-5
2018.6	0.0039	0.0024	0.0155	0.0029	0.0093	0.0098	0.0039	1.8501E-5
2202.1	0.0039	0.0020	0.0151	0.0029	0.0080	0.0094	0.0039	1.3906E-5
2385.6	0.0039	0.0016	0.0147	0.0029	0.0068	0.0091	0.0039	9.3117E-6

Table A.13: Friction Factor (*f*) comparison of different mesh size the 606 fin design.

606 Friction Factor (*f*) Fluent				
Reynolds number	**MS: 1E-03M**	**MS: 5E-04M**	**MS: 1E-04M**	**MS: 8E -05M**
183.5	0.0126	0.0124	0.0699	0.3644
367.0	0.0063	0.0062	0.0350	0.2733
550.5	0.0042	0.0041	0.0233	0.1822
734.0	0.0032	0.0031	0.0175	0.1367
917.5	0.0025	0.0025	0.0140	0.1093
1101.0	0.0021	0.0021	0.0117	0.0911
1284.6	0.0018	0.0018	0.0100	0.0781
1468.0	0.0016	0.0015	0.0087	0.0683
1651.6	0.0014	0.0014	0.0078	0.0607
1835.1	0.0013	0.0012	0.0070	0.0547
2018.6	0.0012	0.0011	0.0064	0.0497
2202.1	0.0011	0.0010	0.0058	0.0456
2385.6	9.7110E-4	9.5031E-4	0.0054	0.0421

Table A.14: Chilton-Colburn Factor (*j*) comparison of different mesh size the 606 fin design.

606 Chilton-Colburn Factor (*j*) Fluent				
Reynolds number	**MS: 1E-03M**	**MS: 5E-04M**	**MS: 1E-04M**	**MS: 8E -05M**
183.5	0.0017	0.0016	0.0039	0.0045
367.0	0.0017	0.0016	0.0039	0.0045
550.5	0.0017	0.0016	0.0039	0.0045
734.0	0.0017	0.0016	0.0039	0.0045
917.5	0.0017	0.0016	0.0039	0.0045
1101.0	0.0017	0.0016	0.0039	0.0045
1284.6	0.0017	0.0016	0.0039	0.0045
1468.0	0.0017	0.0016	0.0039	0.0045
1651.6	0.0017	0.0016	0.0039	0.0045
1835.1	0.0017	0.0016	0.0039	0.0045
2018.6	0.0017	0.0016	0.0039	0.0045
2202.1	0.0017	0.0016	0.0039	0.0045
2385.6	0.0017	0.0016	0.0039	0.0045

Table A.15: Friction Factor (*f*) comparison of different mesh size the 519 fin design.

519 Friction Factor (*f*) Fluent				
Reynolds number	**MS: 8.0E-05M**	**MS: 1.0E-04M**	**MS: 5.0E-04M**	**MS: 1.0E-03M**
171.2	0.1245	0.1183	0.0432	0.0299
342.3	0.0623	0.0592	0.0216	0.0149
513.4	0.0415	0.0394	0.0144	0.0100
684.6	0.0311	0.0296	0.0108	0.0075
855.7	0.0249	0.0237	0.0086	0.0060
1026.9	0.0208	0.0197	0.0072	0.0050
1198.0	0.0178	0.0169	0.0062	0.0043
1369.2	0.0156	0.0148	0.0054	0.0037
1540.3	0.0138	0.0132	0.0048	0.0033
1711.5	0.0125	0.0118	0.0043	0.0030
1882.6	0.0113	0.0108	0.0039	0.0027
2053.8	0.0104	0.0099	0.0036	0.0025
2224.9	0.0096	0.0091	0.0033	0.0023

Table A.16: Chilton-Colburn Factor (*j*) comparison of different mesh size the 519 fin design.

Chilton-Colburn Factor (*j*) Fluent				
Reynolds number	**MS: 8.0E-05M**	**MS: 1.0E-04M**	**MS: 5.0E-04M**	**MS: 1.0E-03M**
171.2	0.00522	0.00583	5.5302E-4	3.8012E-4
342.3	0.00522	0.00583	5.5302E-4	3.8012E-4
513.4	0.00522	0.00583	5.5302E-4	3.8012E-4
684.6	0.00522	0.00583	5.5302E-4	3.8012E-4
855.7	0.00522	0.00583	5.5302E-4	3.8012E-4
1026.9	0.00522	0.00583	5.5302E-4	3.8012E-4
1198.0	0.00522	0.00583	5.5302E-4	3.8012E-4
1369.2	0.00522	0.00583	5.5302E-4	3.8012E-4
1540.3	0.00522	0.00583	5.5302E-4	3.8012E-4
1711.5	0.00522	0.00583	5.5302E-4	3.8012E-4
1882.6	0.00522	0.00583	5.5302E-4	3.8012E-4
2053.8	0.00522	0.00583	5.5302E-4	3.8012E-4
2224.9	0.00522	0.00583	5.5302E-4	3.8012E-4

Table A.17: Friction Factor (*f*) comparison of different mesh size the 635 fin design.

Friction factor (*f*) Fluent			
Reynolds number	**MS: 1.0E-04M**	**MS: 5.0E-04M**	**MS: 1.0E-03M**
145.1	0.3845	0.4825	0.4817
290.3	0.1922	0.2412	0.2409
435.4	0.1282	0.1608	0.1606
580.5	0.0961	0.1206	0.1204
725.7	0.0769	0.0965	0.0964
870.8	0.0641	0.0804	0.0803
1015.9	0.0549	0.0689	0.0688
1161.1	0.0481	0.0603	0.0602
1306.2	0.0427	0.0536	0.0535
1451.3	0.0384	0.0483	0.0482
1596.5	0.0350	0.0439	0.0438
1741.6	0.0320	0.0402	0.0401
1886.7	0.0296	0.0371	0.0371

Table A.18: Chilton-Colburn Factor (*j*) comparison of different mesh size the 635 fin design.

Chilton-Colburn Factor (*j*) Fluent			
Reynolds number	**MS: 1.0E-04M**	**MS: 5.0E-04M**	**MS: 1.0E-03M**
145.1	0.0029	0.0021	1.682E-4
290.3	0.0029	0.0021	1.682E-4
435.4	0.0029	0.0021	1.682E-4
580.5	0.0029	0.0021	1.682E-4
725.7	0.0029	0.0021	1.682E-4
870.8	0.0029	0.0021	1.682E-4
1015.9	0.0029	0.0021	1.682E-4
1161.1	0.0029	0.0021	1.682E-4
1306.2	0.0029	0.0021	1.682E-4
1451.3	0.0029	0.0021	1.682E-4
1596.5	0.0029	0.0021	1.682E-4
1741.6	0.0029	0.0021	1.682E-4
1886.7	0.0029	0.0021	1.682E-4

Table A.19: Friction factor (*f*) comparison of different mesh size the Combination (606 & 635) fin design.

Combination (606 & 635) Friction factor (*f*) Fluent			
Reynolds number	**MS:1.0e-04 M**	**MS: 5.0e-04 M**	**MS:1.0e-03 M**
164.3	0.0674	0.1118	0.0144
328.6	0.0337	0.0559	0.0072
492.9	0.0225	0.0373	0.0048
657.2	0.0169	0.0280	0.0036
821.5	0.0135	0.0224	0.0029
985.8	0.0112	0.0186	0.0024
1150.1	0.0096	0.0160	0.0021
1314.4	0.0084	0.0140	0.0018
1478.7	0.0075	0.0124	0.0016
1643.0	0.0067	0.0112	0.0014
1807.3	0.0061	0.0102	0.0013
1971.6	0.0056	0.0093	0.0012
2135.9	0.0052	0.0086	0.0011

Table A.20: Chilton-Colburn Factor (*j*) comparison of different mesh size the Combination (606 & 635) fin design.

Combination (606 & 635) Chilton-Colburn Factor (*j*)Fluent			
Reynolds number	**MS:1.0e-04 M**	**MS:5.0e-04 M**	**MS:1.0e-03 M**
164.3	0.0039	0.0018	1.8623E-4
328.6	0.0039	0.0018	1.8623E-4
492.9	0.0039	0.0018	1.8623E-4
657.2	0.0039	0.0018	1.8623E-4
821.5	0.0039	0.0018	1.8623E-4
985.8	0.0039	0.0018	1.8623E-4
1150.1	0.0039	0.0018	1.8623E-4
1314.4	0.0039	0.0018	1.8623E-4
1478.7	0.0039	0.0018	1.8623E-4
1643.0	0.0039	0.0018	1.8623E-4
1807.3	0.0039	0.0018	1.8623E-4
1971.6	0.0039	0.0018	1.8623E-4
2135.9	0.0039	0.0018	1.8623E-4